Gisin Aviation Presents:

ADAMANT

A High Altitude Long Endurance Atmospheric Research UAV

2004-2005 AIAA Individual Aircraft Design Competition

Yevgeniy Gisin

California Polytechnic State University, San Luis Obispo

Abstract

Gisin Aviation is proud to present *Adamant* – the response to the Request for Proposal (RFP) presented in the 2004/2005 AIAA Individual Aircraft Design Competition. The aircraft is a long-endurance high-altitude Uninhabited Air Vehicle (UAV) with a primary role of hurricane reconnaissance. *Adamant* is a twin-boom aircraft of 10,400 lb takeoff gross weight powered by a 2,700 horsepower advanced turboprop engine. The aircraft has a 1,500 nmi. mission radius, and is designed for a 48-hour long time-on-station (TOS) at an altitude of 45,000ft and a 32-hour long TOS at an altitude of 65,000 ft.

A UAV design was specified in the RFP in order to reduce the risk associated with hazardous and tedious patrol tasks, maximize the airframe's performance capability, and decrease mission cost. One of the primary foci of this design is high modularity, which allows *Adamant* to be easily modifiable to perform a wide range of alternate missions. The distinguishing features of the aircraft – the removable payload section and the quadricycle landing gear – both greatly contribute to such mission flexibility. The "twin-barrel" engine configuration allows for twin-engine safety to be obtained in a one-propeller airframe.

The design qualities and performance capabilities of *Adamant* allow it to perform weather reconnaissance and other high-altitude long-endurance missions for both civilian and military customers in a low cost, safe and efficient manner. *Adamant* is therefore an optimum solution to the requirements presented in the RFP.

Table of Contents

1. Introduction 1

2. RFP Discussion 2

3. Weather Reconnaissance Mission and Hale Aircraft Analysis 4

    3.1 Weather Reconnaissance Mission 4

    3.2 Evaluation of Existing Aircraft 5

4. Initial Sizing 7

5. Configuration 10

    5.1 Aerodynamic Configuration 10

    5.2 Chosen Configuration 12

6. Aerodynamics 16

7. Performance 19

8. Propulsion 22

9. Propeller Sizing 27

10. Weight and Balance 30

11. Stability and Control 32

12. Structures and Materials 36

13. Landing Gear 42

14. Fuel System 44

15. Alternate Missions and Payload Systems 46

16. RFP-Specified Systems 49

17. System Operations 51

    17.1 Vehicle Control 51

    17.2 LEO Satcom Antenna 53

    17.3 System Deployment Considerations 56

18. Cost Estimation 58

19. Validation Model 60

Appendix 1 65

Appendix 2 68

References 71

Table of Tables

Table 1 – Desirable Qualities.. 6
Table 2 – Induced Drag of Various Configurations... 11
Table 3 – Propeller Performance 28
Table 4 – Aircraft Weight Breakdown.. 30
Table 5 – *Adamant* Control Derivatives 35
Table 6 – Payload Clearances 49
Table 7 – Operations Costs Breakdown.. 59
Table 8 – RFP Requirements Compliance Matrix 64

Table of Figures

Figure 1 – Mission Profiles 2
Figure 2 – Current Generation HALE Aircraft 5
Figure 3 – Turboprop/Turbojet Sizing Maps 8
Figure 4 – Turboprop Sizing Map 9
Figure 5 – Sufrace Configurations Considered 10
Figure 6 – Eppler 431 Airfoil 16
Figure 7 – Airfoil Performance (Re=3,000,000) 17
Figure 8 – XLFR5 Results 18
Figure 9 – Aircraft Drag Breakdown 19
Figure 10 – Thrust vs. Drag Plot 20
Figure 11 – Climb Rates 20
Figure 12 – Takeoff and Landing Diagrams 21
Figure 13 – Rolls Royce CTP800-4T 22
Figure 14 – Straight-through Engine Installation 23
Figure 15 – PT6 Reverse Flow Turboprop Engine 24
Figure 16 – Reverse Flow Engine Installation 25
Figure 17 – CTP800-4T Engine Installation 26
Figure 18 – Propeller Sizing Output 27
Figure 19 – Propeller-to-Boom Clearance 29
Figure 20 – Aircraft CG Excursion 31
Figure 21 – Control Surfaces 32
Figure 22 – Control Volume Coefficients 33
Figure 23 – Geometry for AVL Analysis 34
Figure 24 – Aircraft Structural Configuration 36
Figure 25 – Materials Usage 38
Figure 26 – Wing Spar Lay-up 39
Figure 27 – V-n Diagram 40
Figure 28 – White Knight Landing Gear Configuration 42
Figure 29 – Landing Gear Retraction Geometry 43
Figure 30 – Fuel Tank Configuration 44

Figure 31 – Payload Section Removal ... 46
Figure 32 – Aerodynamic Payload Fairing Modification ... 47
Figure 33 – Underslung Customer-Configured Payload ... 48
Figure 34 – RFP-Specified Systems Clearances ... 49
Figure 35 – Predator System Operational Schematic ... 52
Figure 36 – Predator A Internals ... 54
Figure 38 – Luneberg Lens Antenna Installation ... 55
Figure 39 – Cost versus Production Run Size ... 58
Figure 40 – Validation Model ... 60
Figure 41 – Flight Testing Video Captures ... 61

Foldouts

Foldout 1 – Aircraft 3-View ... 14
Foldout 2 – System Features ... 15

Nomenclature

AR	Aspect Ratio
C_D	Drag Coefficient
CG	Center of Gravity, ft, in
C_L	Coefficient of Lift
C_l	Section Coefficient of Lift
C_M	Moment Coefficient
FOD	Foreign Object Damage
L/D	Lift to Drag Ratio
M	Mach Number
MAC	Mean Aerodynamic Center, ft
OEI	One Engine Inoperative
OEW	Operating Empty Weight
RFP	Request for Proposal
Re	Reynolds Number
SFC	Specific Fuel Consumption, lb/lb/hr
S_{ref}	Wing Reference Area, ft^2
S_{wet}	Wetted Area, ft^2
S_{TS}	V-tail True Surface Area, ft^2
S_{HT}	Horizontal Tail Surface Area, ft^2
S_{VT}	Vertical Tail Area, ft^2
TOGW	Takeoff Gross Weight, lb
V	Velocity, fps, kts
W/S	Wing Loading, lb/ft^2
c	Wing Chord, ft
e	Oswald Efficiency Factor
t/c	Thickness to Chord Ratio
α	Angle of Attack, deg
δ	Control Surface Deflection, deg
ρ	Density, $slug/ft^3$

1. Introduction

Hurricanes have always been known as one of the most terrible natural disasters that can befall a community. Modern forecasting methods have allowed a reduction of the danger hurricanes present to humans, but they still cause many deaths and billions of dollars of damage, attacking the US mainland with regularity. Weather reconnaissance, while neither a very glamorous nor a well-known aircraft mission, is a crucial component in preventing such tragedies. Weather reconnaissance can save lives by accurately tracking hurricanes and can advance atmospheric science by taking measurements of wind speed and direction within a hurricane.

A variety of aircraft have been used throughout the years for this task. The well-known 53rd Weather Reconnaissance Squadron of the U.S. Air Force has flown a variety of military aircraft including the B-17 and the B-47. Currently, the mission is accomplished by modified C-130 *Hercules* and P-3 *Orion* aircraft.

Mission endurance has always been one of the limits to the productivity of such aircraft, with crew endurance oftentimes being a more stringent constraint than fuel available. Higher vehicle endurance would not only enable more thorough weather system analysis, but also make the overall mission cheaper and more efficient. This existent need and the recent maturity of UAV technology make these aircraft attractive to the hurricane-hunting mission. The goal of the study described in this paper was to create an answer to this requirement – a mission-adaptable UAV with a primary goal of hurricane reconnaissance.

2. RFP Discussion

The RFP specifies two missions, which can be seen in detail in Figure 1. Both missions are flown with the same payload, with the same range, and the same divert requirements. The two missions differ in loiter altitudes and time-on-station, with the first mission requiring a 32-hour TOS at 65,000 ft and the second mission requiring a 48-hour TOS at 45,000 ft.

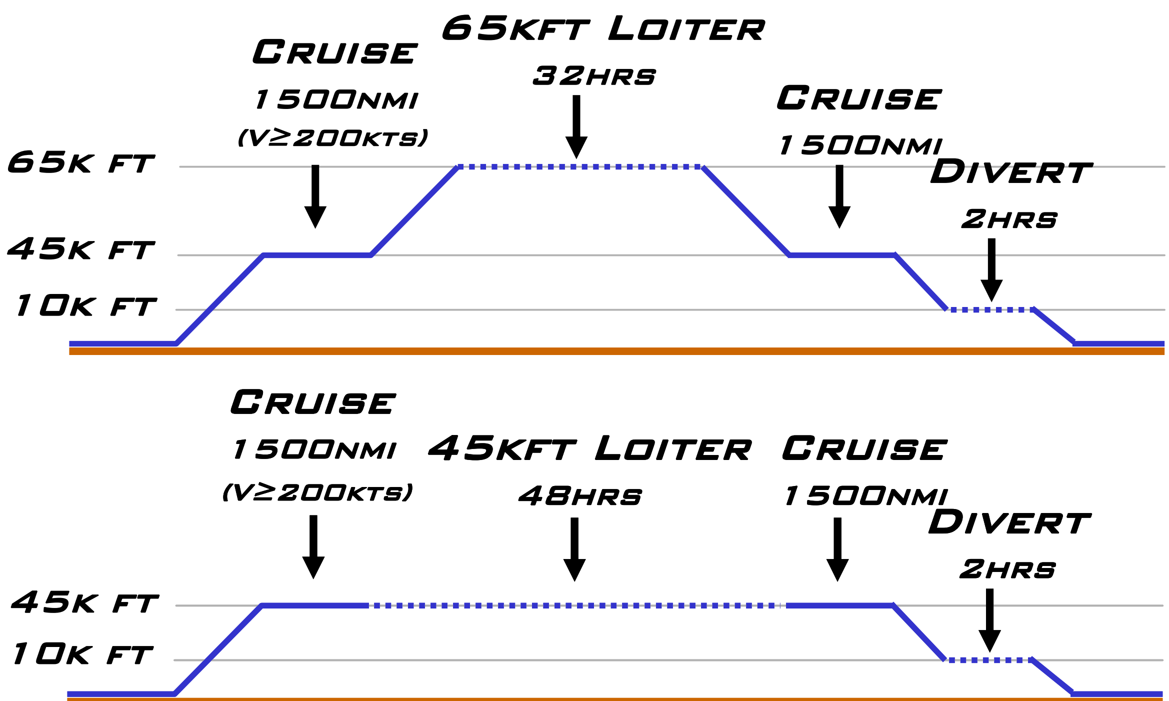

Figure 1 – Mission Profiles

The deployable payload specified for the mission is comprised of 72 Vaisala RD93 dropsondes, with a total variation of payload weight being approximately 62 lbs. A number of other support systems are also specified in the RFP, increasing the total payload weight to 852 lbs.

The RFP allows for a decrease in loiter time and payload capacity if such a decrease is warranted by an increase in overall mission efficiency. This did not prove to be a favorable tradeoff. Having performed a sizing trade study for lower-payload aircraft, it was clear that the maximum-capacity UAV was the cheapest way to accomplish the RFP's 2,000 flight hours per year on-station goal.

The RFP mission requires a rapid response to a hurricane weather system, something that is disallowed by current FAA regulations. For example, the *Global Hawk* UAV team is required to file a flight plan with the FAA 7 days in advance of a mission. Such a requirement is sure to prohibit the RFP's primary mission, so it is assumed that changes will occur to the regulations in time for a UAV to be able to perform this mission as intended. Recent NASA research[1] under the auspices of the ERAST program shows that development of technologies that will enable this change is well under way.

The RFP describes a prospective need for only 10 hurricane-hunter UAVs to exist in the constraints of today's government budget. This is decidedly too low of a production quantity to allow for a development of an entirely-new vehicle. For this reason, the RFP places a heavy import on the additional modularity and mission-adaptability requirement specified for this vehicle. If the development of such a system is to be warranted, the aircraft must be able to bring new capabilities to a wide range of customers and be able to secure a much larger buy size.

3. Weather Reconnaissance Mission and Hale Aircraft Analysis

3.1 Weather Reconnaissance Mission

The weather reconnaissance mission emanated from the need of military commanders to know with high certainty the expected weather conditions at the field of battle. Balloons, ground stationed meteorologists, aircraft and satellites have all been used to gather information on weather phenomena. Accurate weather forecasts are paramount to military action, and many a military success or failure, like the Invasion of Normandy in 1944, depended on accurate forecasts.

Starting in World War 2, driven by the vital need for accurate weather information, the US military started forming dedicated weather reconnaissance squadrons. In 1944, four B-25s were assigned to the "Army Hurricane Reconnaissance Unit", which can be considered the forerunner of today's "Hurricane Hunters". Because of the availability of specialized equipment and trained personnel, it was only natural that the task of weather reconnaissance would be taken up by the military during peacetime as well. The weather services of the military, in particular the specialized "Hurricane Hunters" squadron have been researching and tracking various weather phenomena for decades.

Until recently, measurements that could be taken by weather research aircraft were relatively limited, being restricted to the data of on-board sensors. Recently developed expendable parachute-droppable sondes have added a new degree of precision to the data that can be collected. With a GPS system, a data uplink and a set of instruments onboard, the sondes send position and sensor readings up to the science aircraft. Given the cost and safety benefits of UAV platforms and their proliferation into many areas previously reserved for manned aircraft, it is easy to see them becoming the next step in increasing the capabilities of our weather reconnaissance assets. Although seemingly unglamorous, the weather reconnaissance mission has an extremely important one, and in one way or another has affected all of us. Increasing the capabilities of the weather reconnaissance forces is sure to result in a decrease in hurricane damage and improve our scientific knowledge.

3.2 Evaluation of Existing Aircraft

An evaluation of a number of other aircraft that are designed to perform a high-altitude long-endurance mission was conducted. The performance of these aircraft was assessed to see if any could perform the mission of the RFP, and their desirable characteristics were evaluated to see if they could be incorporated in the new design. These aircraft are shown in Figure 2, and include the Scaled Composites *Proteus*, General Atomics *Mariner*, Grob *Strato IIC* and Northrop Grumman *Global Hawk*.

Figure 2 – Current Generation HALE Aircraft

Proteus and *Mariner* could not perform the mission of the RFP, first being limited in loiter time and the second in maximum altitude. Grob *Strato IIC* could theoretically perform the mission, but it is a large manned aircraft and is not being produced. *Global Hawk* is also significantly larger than an ideally-sized aircraft for the mission and is quite expensive. It was determined that none of these aircraft could cheaply perform the mission, but a number of lessons were learned from evaluating their configurations. In order for the new design's configuration to synergistically support the overall aircraft mission, a number of important characteristics for this aircraft to possess were defined from both the RFP requirements and evaluation of comparable aircraft. These characteristics are listed in Table 1.

Table 1 – Desirable Qualities

Desirable Characteristic
Low cruise drag
Low in-flight CG shift
Mission adaptability/convertibility
Easy maintenance
Easy access to payload compartment
A way to increase drag in landing configuration

Having determined the general goals and desirable qualities for the new aircraft design, it was decided to ascertain the size of the aircraft prior to picking a definite configuration.

4. Initial Sizing

Initial sizing of the aircraft was performed using a sizing code written in Microsoft Visual Basic, with a Microsoft Excel front-end allowing the user to easily modify all key trade-study parameters. The sizing code is a point-design code, taking a given aircraft configuration and flying the configuration through a specified mission.

Using modular components, the code calculates all of the relevant flight parameters at small time increments throughout all mission segments. The mission segments are goal-based, which allows for aircraft performance to be calculated at optimum conditions, such as flight speeds and climb rates. One of the particulars of the code is its use of real manufacturer-provided engine maps coupled to a 4-dimensional interpolation routine to calculate the engine performance and fuel consumption during flight. Being able to find SFC at a given power level, Mach number, and altitude allows for higher fidelity flight performance estimation. Yet more accuracy is added to the simulation by the Reynolds number-dependent parasite drag routine, which recalculates C_{Dp} at each simulation data point.

The initial question answered by the sizing code was that of propulsion selection. Two studies were run for the 48-hour mission specified in the RFP, one for a turboprop-powered and the other for a turbojet-powered aircraft. This trade and the resultant sizing difference between the optimum solutions for the two aircraft can be seen in Figure 3.

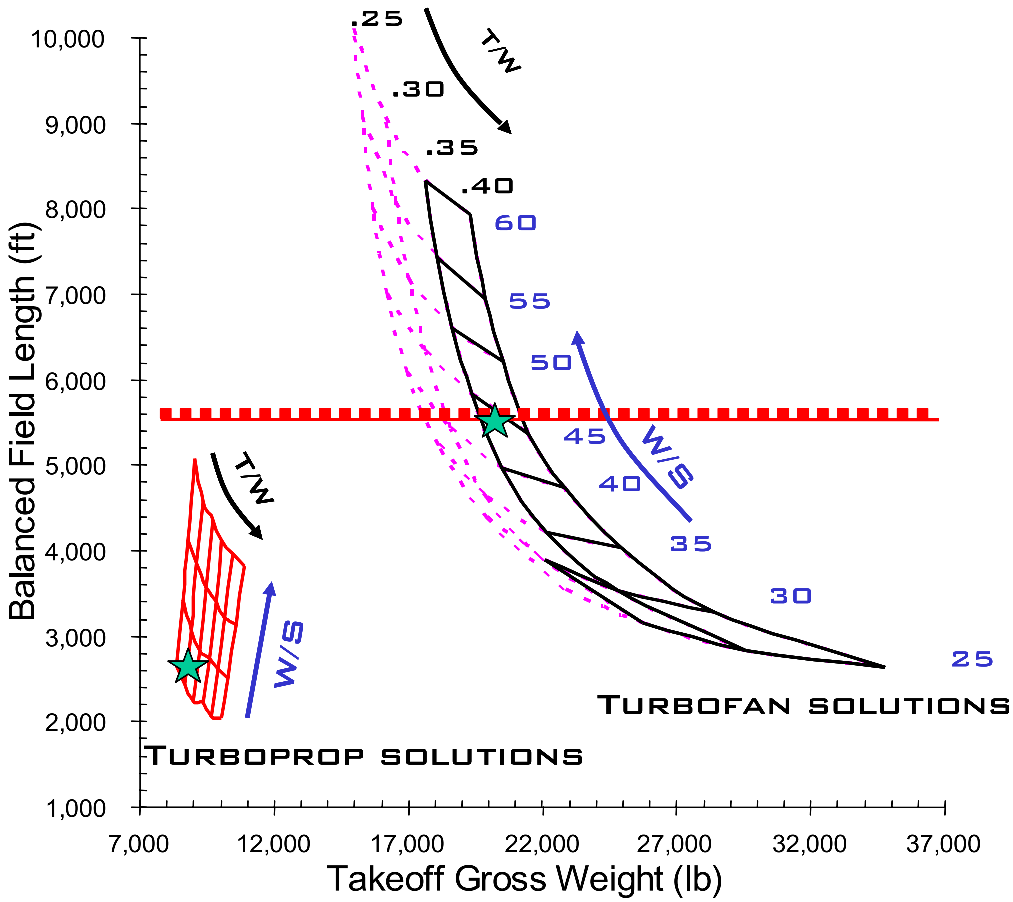

Figure 3 – Turboprop/Turbojet Sizing Maps

The takeoff gross weight difference between optimum turboprop and turbojet solutions varies by approximately 10,000 lb. With weight being a prime driver of aircraft cost, it was judged wise to go on with the development of a turboprop-powered solution.

Having chosen a propulsion system type to be used on *Adamant*, more detailed sizing of a turboprop configuration could proceed. A sizing map of this configuration, displayed in Figure 4, shows how the two major constraints on the RFP mission size the aircraft.

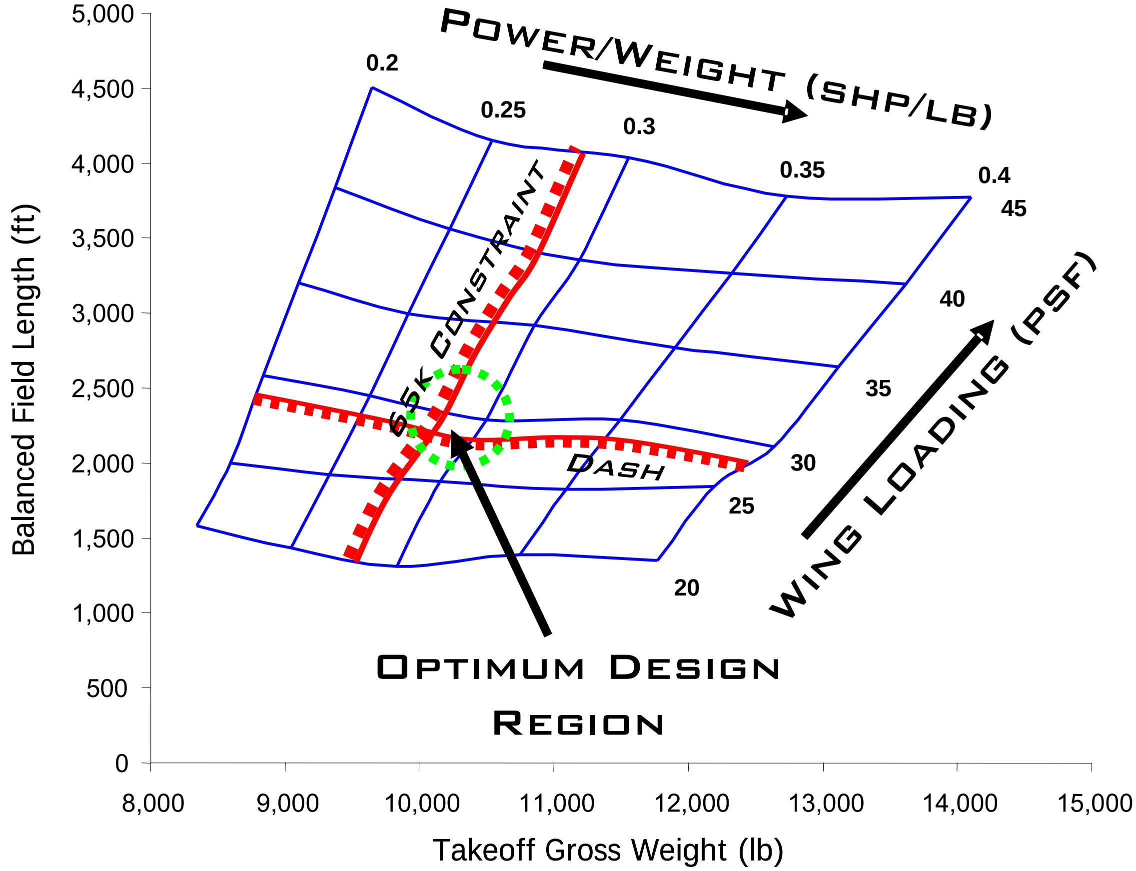

Figure 4 – Turboprop Sizing Map

It can be seen that the lower wing loading aircraft will not be able to meet the 200-knot minimum dash speed constraint of the RFP. Although those aircraft could obviously fly at that speed, they would be flying at a non-optimum point, and thereby drive up aircraft weight. It can also be seen that the configurations with low installed thrust-to-weight ratios are unable to fly a mission at 65,000 ft altitude, losing engine power to altitude-induced thrust lapse. The optimum sizing point is located at the minimum possible weight, and is shown to be approximately 10,000 lb. It is important to note that the turboprop solutions appear not to be sized by, or strongly limited by, the takeoff field constraint.

5. Configuration

5.1 Aerodynamic Configuration

One of the most important characteristics of any aircraft is the arrangement of the aerodynamic surfaces. This choice affects all aspects of the aircraft from controllability and flight performance to aesthetics and cost. A number of flying surface configurations (flying wing, joined-wing, e.t.c.) were initially considered. The final configurational choice is usually made qualitatively by the designer by evaluating the tradeoffs between the pros and cons of each configuration. The configurations considered in this downselection can be seen in detail in Figure 5.

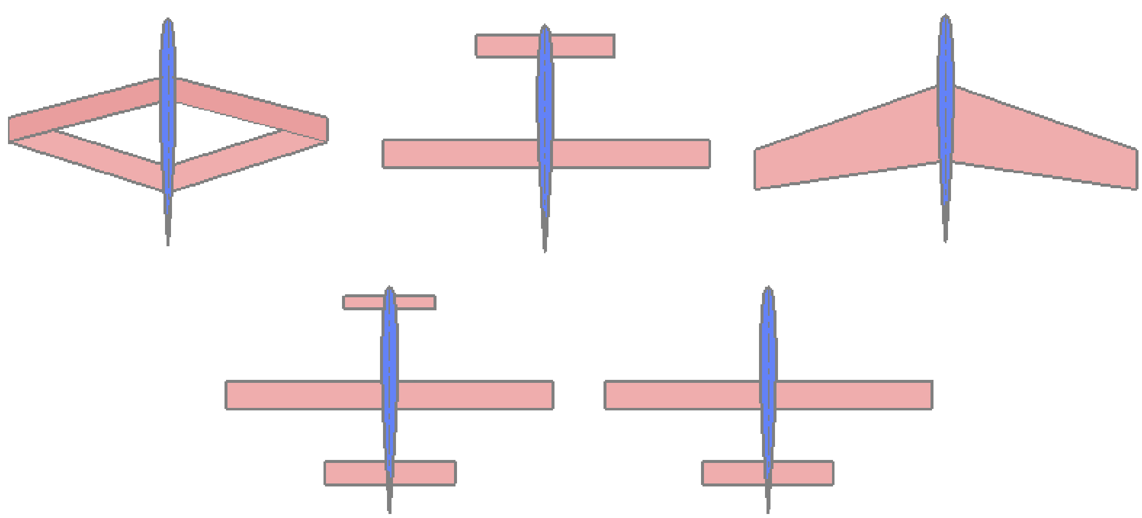

Figure 5 – Sufrace Configurations Considered

The **joined-wing** configuration was eliminated because it did not appear to offer any significant benefits in the mission, while being a challenging concept to realize. The structural benefits of the configuration are sure to be offset by both the research required to make such a configuration viable, and also by the difficult problem presented by the airframe aerodynamic/structural coupling.

The **flying wing** configuration offered certain attractive features in likely possessing the lowest wetted area out of all of the designs. However, with the RFP requirement of modularity and the RFP mission being conducted in unsteady atmospheric conditions, the flying wing also held a number of significant disadvantages. With the payload section being internal to the integrated fuselage/body, the modularity of the design was sure to be reduced. Because of the short control arm afforded to the effective pitch control surfaces, and the resultant low pitch damping and stability, flight in disturbed air conditions, or flight with surface icing would both prove challenging. Because of these reasons, the flying wing configuration was discarded as well.

After evaluation of all possibilities, the choice for the configuration was limited to three alternatives: Three-surface, conventional and canard. A large distinction between these configuration types exists in their trimmed condition induced-drag characteristics. The following table was obtained from a text by Eric R. Kendall of the Gates Learjet Corporation[2].

Table 2 – Induced Drag of Various Configurations

Configuration	CG Location	
	Aft	Fwd
Three-Surface	1.000	1.000
Conventional	1.006	1.069
Canard	1.229	1.316

It could be seen that the canard configuration was a losing one from the viewpoint of induced drag, while the conventional and three-surface configurations each had their benefits. When considering that the advantages of a three-surface configuration are best applied to aircraft with a widely-variable CG location, high maneuvering requirements, or payload integration issues, the conventional configuration seemed to be the most logical choice.

On initial evaluation of the RFP, it was noticed that the deployable payload specified in the mission represented a very small fraction of the overall weight of the aircraft. This low deployable payload weight could permit the payload compartment to not coincide with the CG of the aircraft, thereby enabling significant freedom in configurational evolution. Two components of the aircraft weight changed during the mission. With the in-mission fuel weight being approximately 50 times heavier than that of the expended payload, the fuel was considered a much more important weight component to locate on the CG of the aircraft.

An important way to decrease the parasitic drag of the aircraft is by encouraging laminar flow on as much of the wetted surface of the airframe. Laminar flow is likely to be achievable on the smooth surfaces produced with composite materials, and by the fact that most of the mission is conducted at altitudes above those where collisions with insects and dust can affect the surface finish. Another way to encourage laminar flow is by locating as much of the airframe outside of the wake of the propeller, which tends to be more turbulent than the freestream airflow. As such, a pusher configuration is likely to hold a benefit to the configuration.

5.2 Chosen Configuration

The final aircraft is a conventional aerodynamic configuration and is powered by a pusher turbo prop engine. The nose section of the aircraft is removable in order to allow for easy mission modularity. The aircraft underbody is clear of landing gear or gear retraction trajectories, therefore becoming an ideal location for installation of external on-CG payloads. The quadricycle landing gear allows the aircraft to remain stable on the ground with the nose section removed, and also allows for easy maintenance and installation access to the underbody of the aircraft.

Adamant is controlled in pitch and yaw by a “separated V-tail”, which is composed of two separate control surfaces angled at 40° from the horizontal. A variety of reasons exist for why these two tail surfaces are not connected. The attempt was made to reduce aerodynamic drag by keeping as much of the aircraft surface away from the propeller-disturbed airflow. According to an early calculation, a TOGW decrease of approximately 100lbs could be achieved by maintaining laminar flow on the tail surface. Other benefits included mold-sharing possibilities for the two tailbooms, lack of structural coupling between the two surfaces/booms, and finally the pleasing aesthetics of such a configuration. Considering that a reversion to either an inverted V-tail or an H-tail would not be difficult to implement in a later stage of the design, and that a number of successful aircraft with unconnected tail surfaces exist, this tail configuration appeared to have enough merit to implement on *Adamant*.

One of the peculiarities of high lift-to-drag aircraft such as *Adamant* occurs during landing. These aircraft tend enter ground effect early and have difficulties slowing down to alighting speeds, floating down the runway. A method to generate drag on landing was necessary to be implemented, and had to be considered during configuration definition. As a solution, *Adamant*’s propeller installation will also be used to generate the required amounts of drag on landing by short-pitching the propeller

Item	Weight (lbs)	Station (in)
Fuselage	326	160
Main Wing	508	147
Landing Gear	197	148
Engine	1,197	229
Engine Installation	390	215
Vertical 1	63	360
Vertical 2	63	360
Fuel System	373	150
Engine Start	29	225
Avionics	525	113
Tailbooms	285	200
Fuel Dump	20	170
Flight Controls	331	147
Air Induction	123	210
Electric System	264	147
Mission Payload	852	61
Fuel	4,800	162

Weight Empty	**5,546 lbs**
Takeoff Gross	**10,346 lbs**
Quarter Chord	**158 in**
Rear Limit	**171 in**

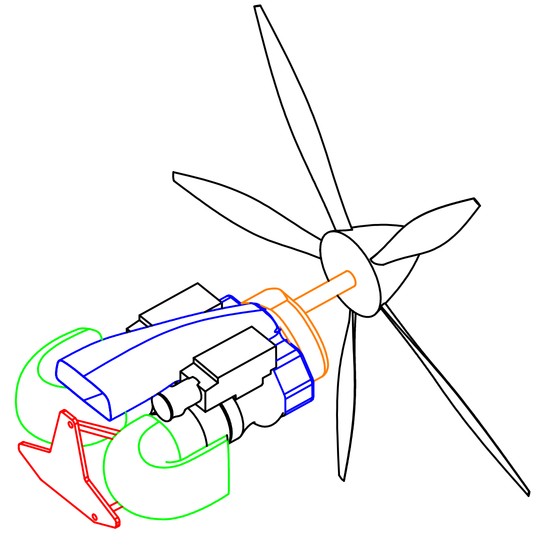

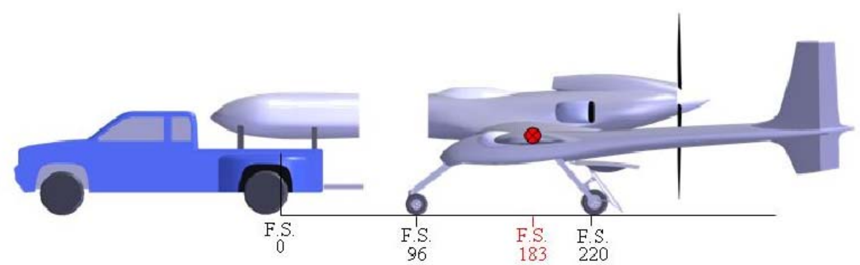

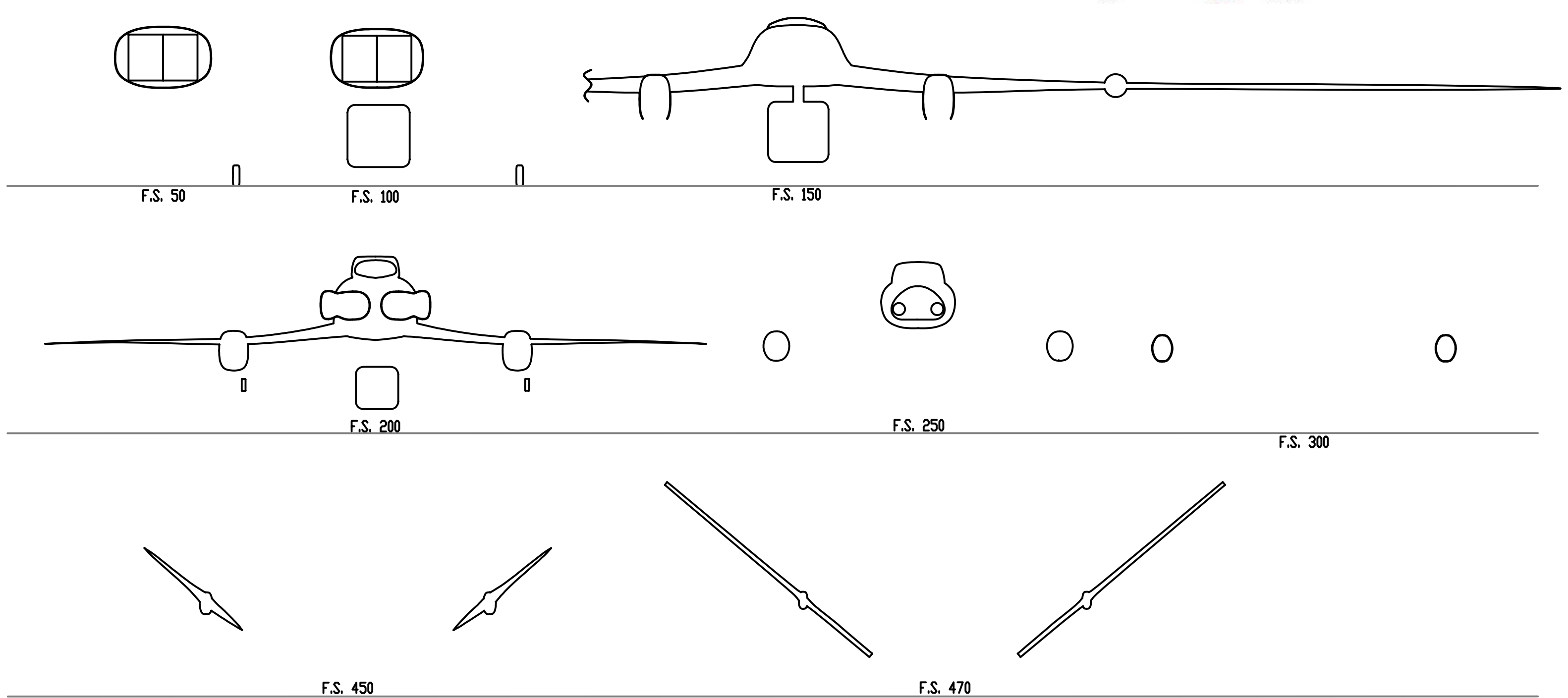

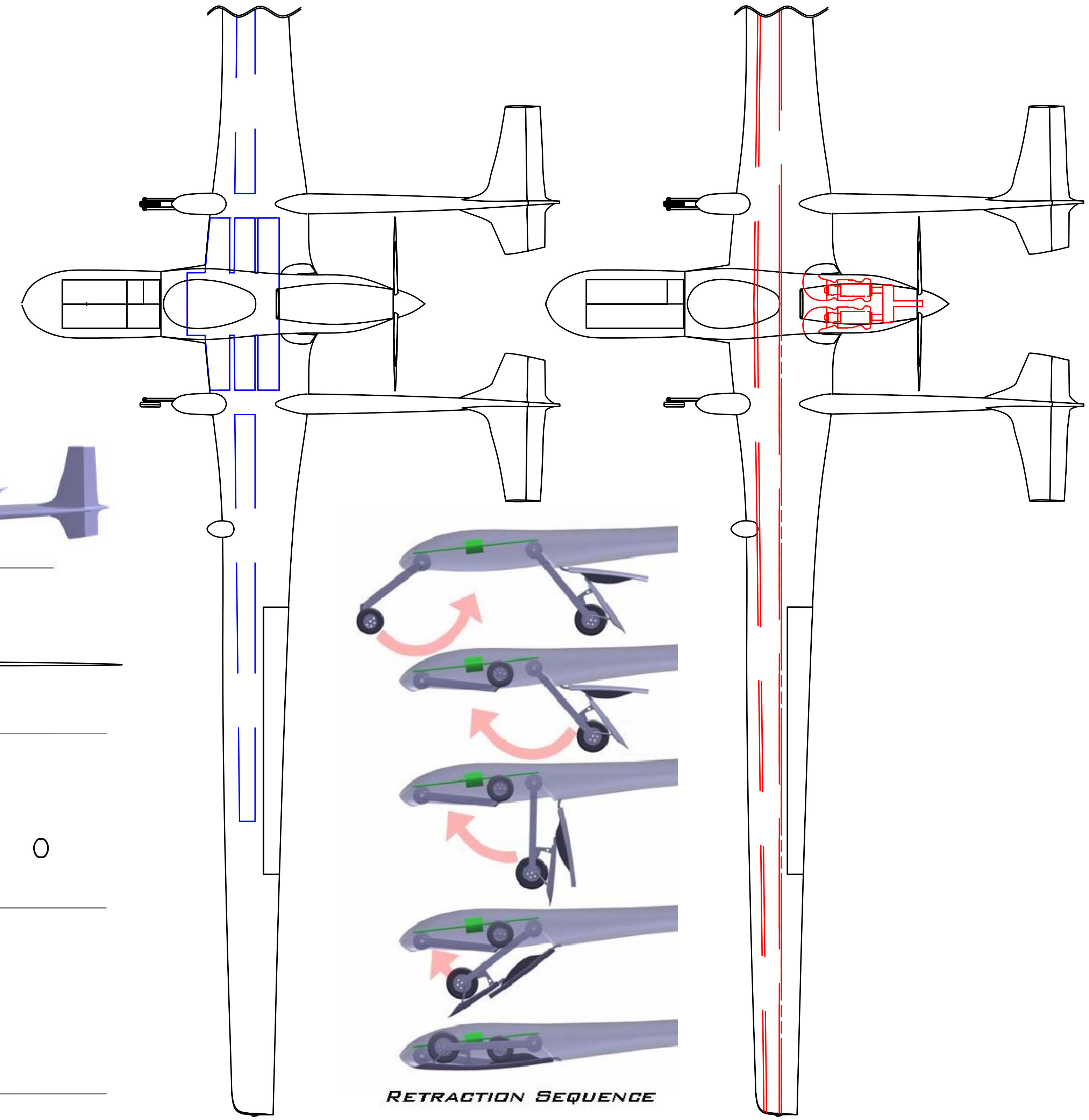

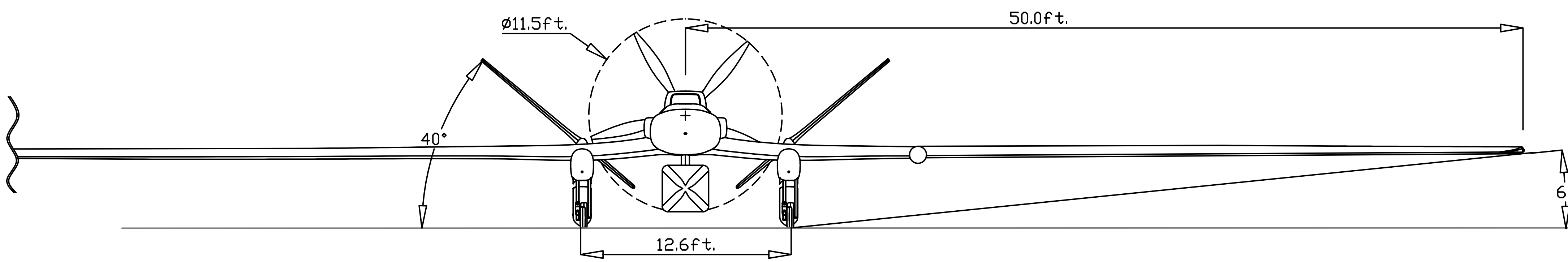

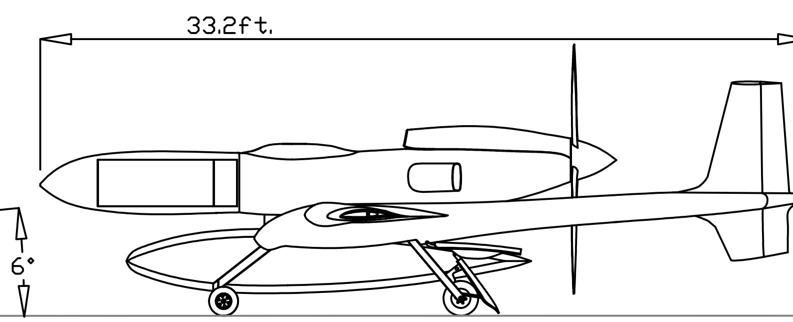

DATE:	SCALE:	DRAWING NAME:	DRAWN BY:
05/29/2005	1:100	Adamant	Yevgeniy Gisin

Fuselage Inboard

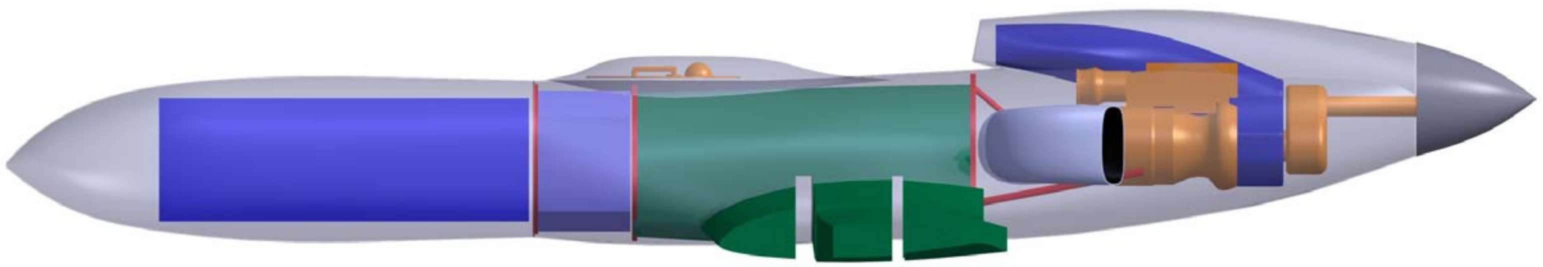

No propeller wake on airframe

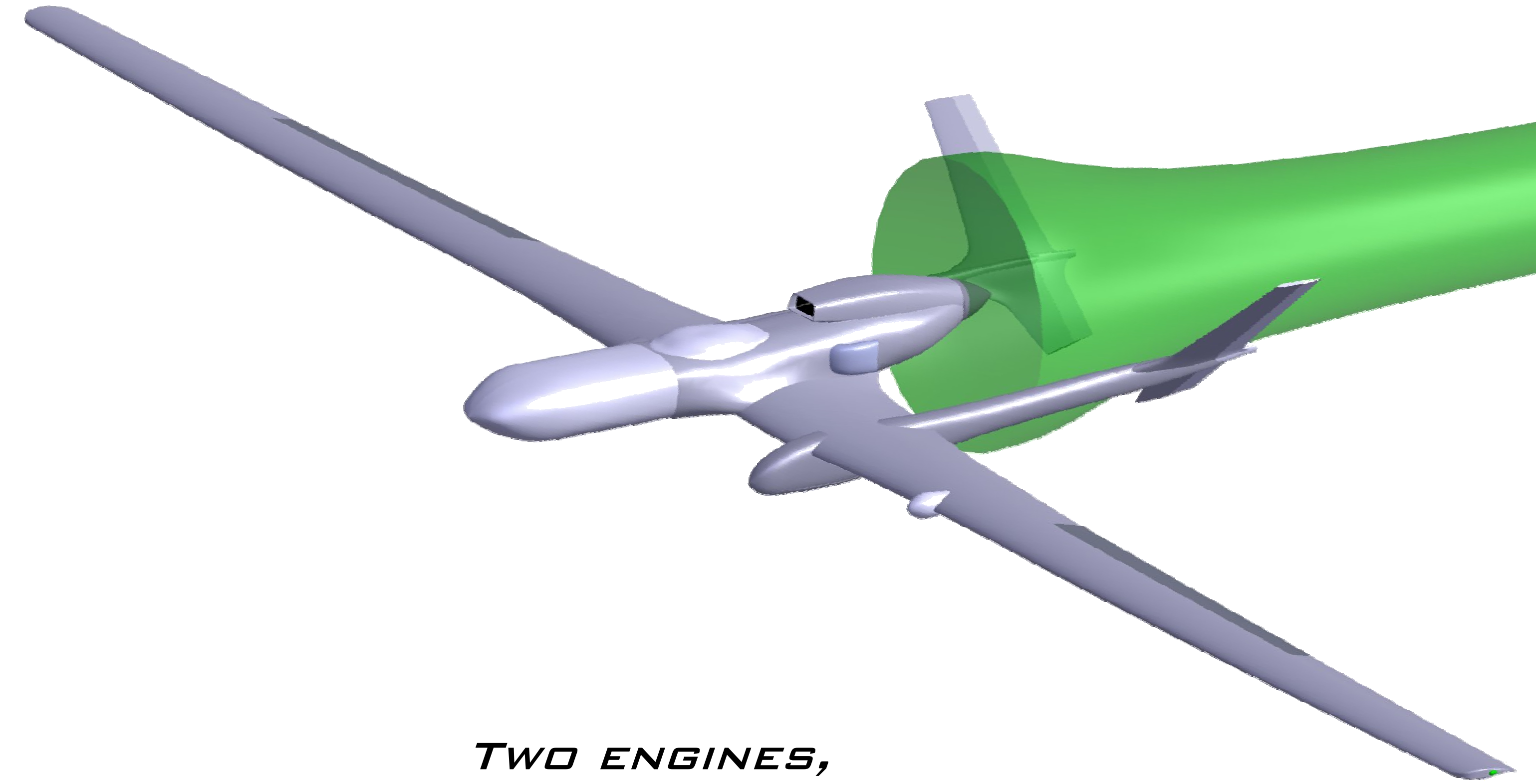

ADAMANT

Wing Area	380 ft^2	**Takeoff Gross Weight**	10,400 lb
Aspect Ratio	27 -	**Empty Weight**	4,690 lb
Mean Aerodynamic Chord	4.16 ft	**Fuel Weight**	4,800 lb
Wing Span	100 ft	**Wing Loading**	27 psf
Installed Power	2,700 hp	**Maximum L/D Ratio**	36 -

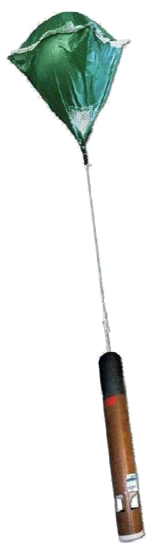

RFP Mandated Payloads:

Item	Weight	Quantity
Vaisala RD93 Dropsonde	0.86	72
Dropsonde Container	200	1
Dropsonde Data System	90	1
Mission Equipment	500	1
Total:	852 lbs	

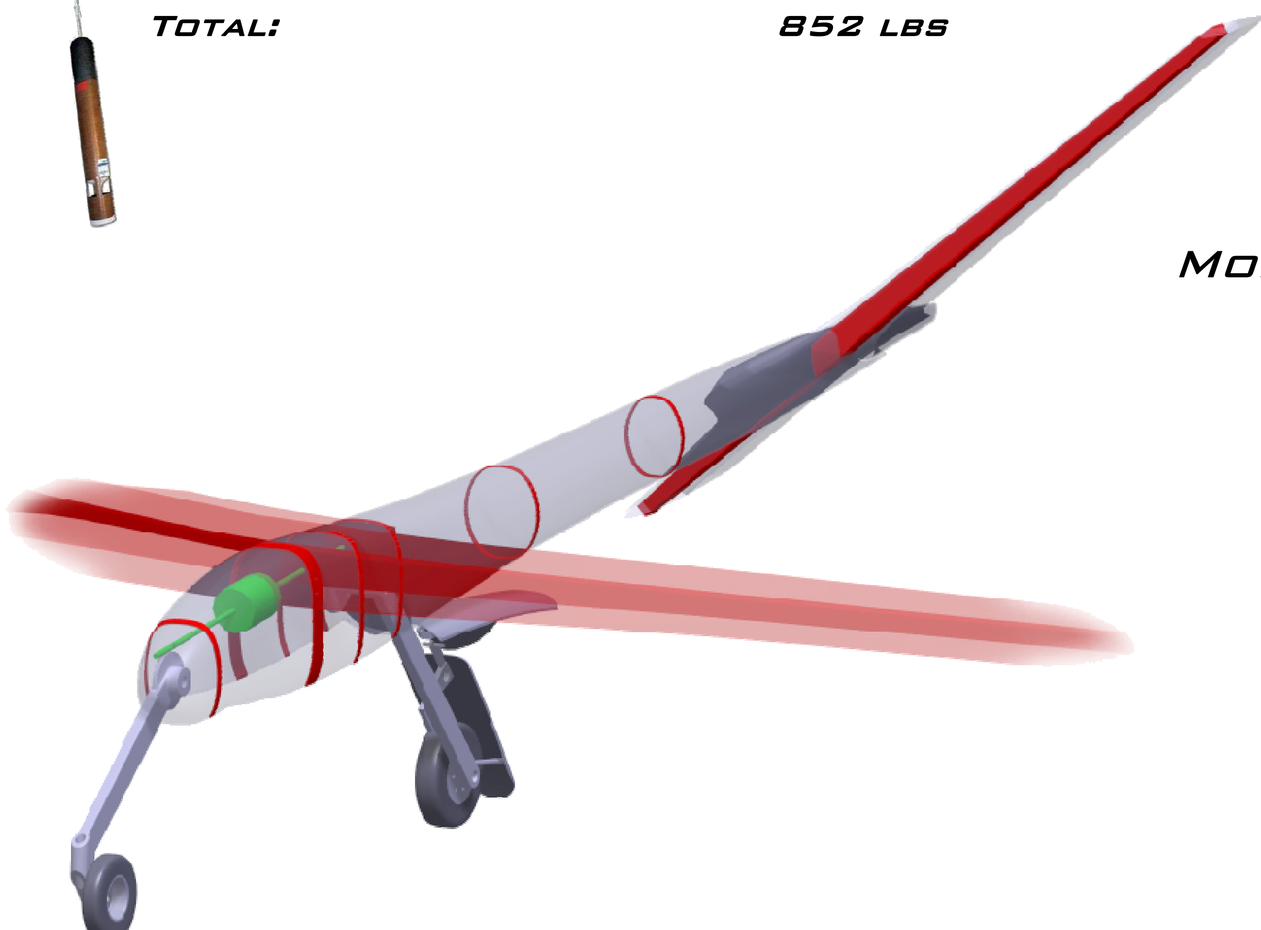

Landing Gear Installation

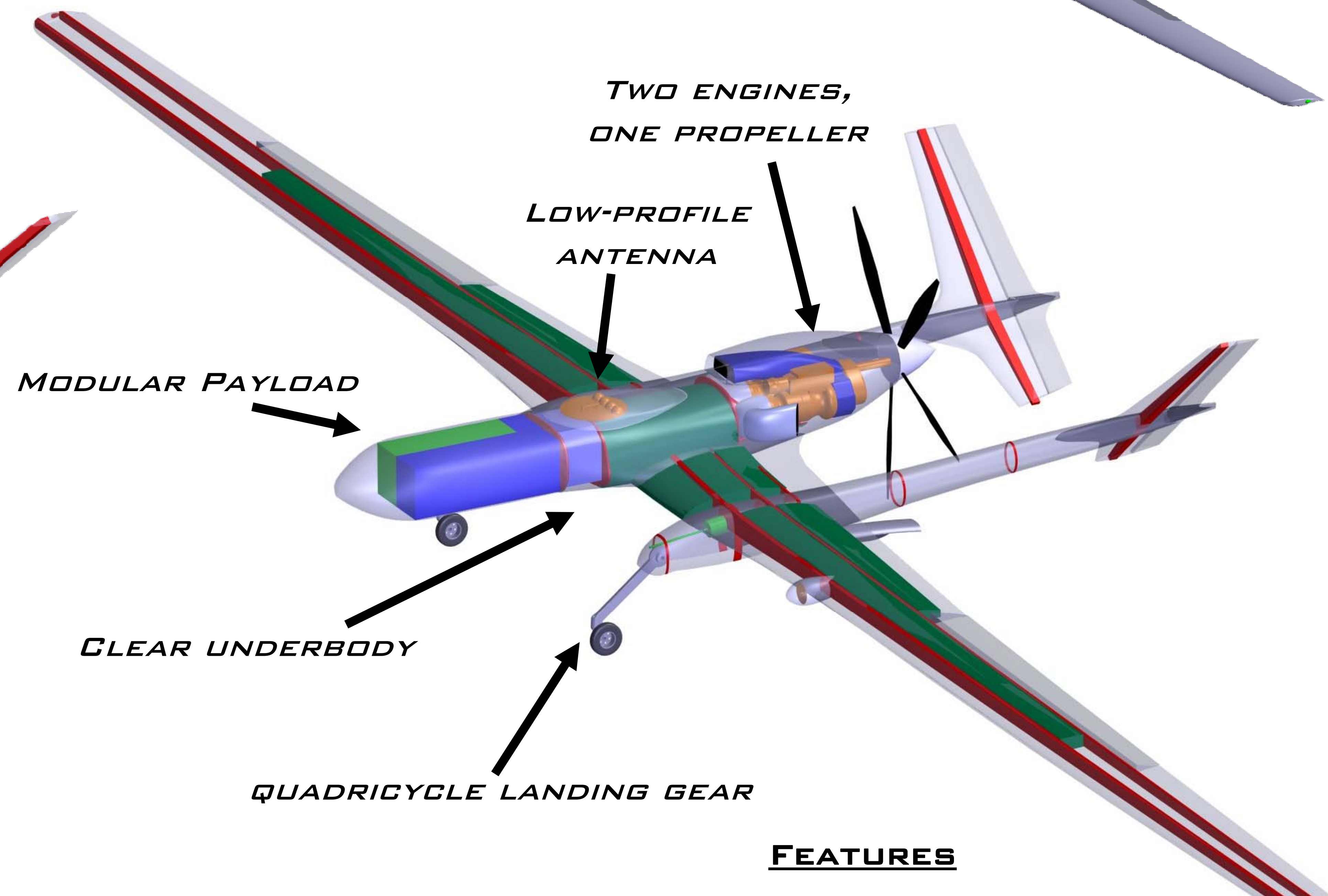

Features

6. Aerodynamics

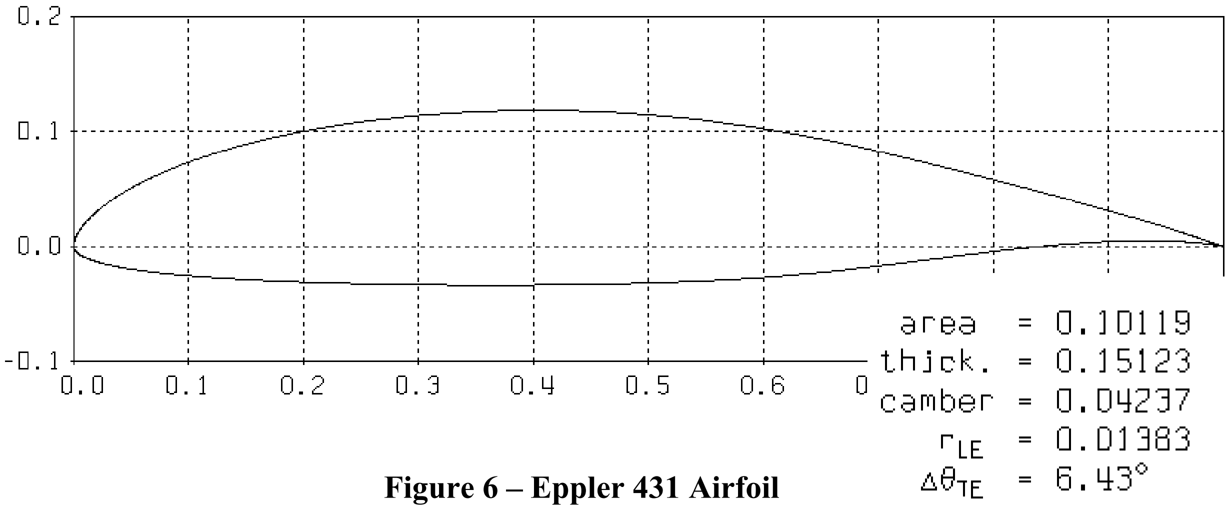

Figure 6 – Eppler 431 Airfoil

The Eppler 431 airfoil was chosen for the wing for a variety of reasons. Most importantly, the airfoil is designed to maintain laminar flow over much of its surface, which allows it to possess a low coefficient of drag at the cruise C_L condition. With the airfoil being 15% thick, the wing has large amount of internal volume for fuel storage. The high thickness of the airfoil also allows for the wing to achieve the required structural rigidity while using more efficient, lighter spars. Mach-induced drag rise in high-thickness airfoils is not a concern, considering that the mission of the aircraft is conducted at low subsonic flight speeds.

The airfoil performance was analyzed using the XFOIL code at Reynolds numbers representative of loiter flight at an altitude of 45,000 ft and is shown in detail in Figure 7. The lift curve shows a gradual stall behavior and an operating/cruise point far away from stall. The drag polar shows that the airfoil is still comfortably within its drag bucket at the cruise lift coefficient. All of these performance characteristics are favorable for the high-altitude long endurance mission, making the E431 a good final airfoil choice.

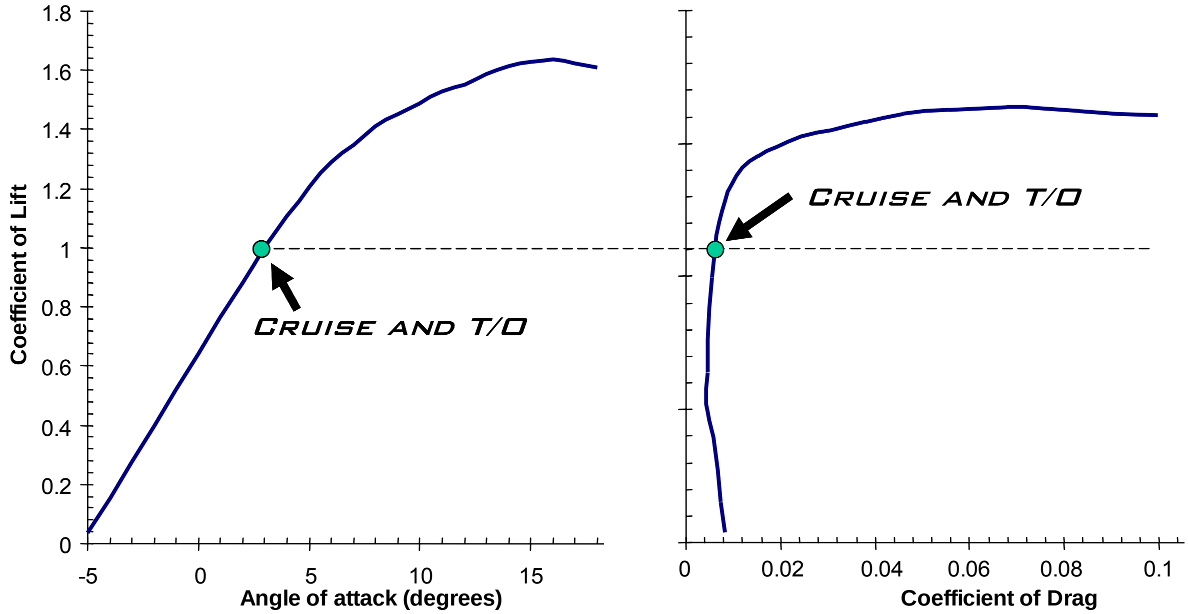

Figure 7 – Airfoil Performance (Re=3,000,000)

It is important to design the wing planform to minimize induced drag. Increasing the wing aspect ratio is one of the methods to do this; however, the structural disadvantages of high aspect ratio wings slowly start to outweigh the benefits offered by the low induced drag. Aerodynamic tailoring of the airfoil cross-sections spanwise is a second method to obtain higher efficiency in a wing configuration, without creating any structural problems. This is achieved by either geometric twist (changing the angle of attack of the airfoil sections at different span-wise datum points on the wing), or by aerodynamic twist (variation of airfoil section geometry at different span-wise datum points on the wing). Because the resultant washout also has a beneficial effect on the aircraft stall characteristics, this type of planform tailoring was chosen to be used.

The wing twist distribution was tailored using a lifting-line theory code called XFLR5[3]. This code uses classical lifting-line theory equations and couples these with airfoil performance values obtained from the XFOIL[4] viscous boundary layer airfoil analysis code developed by Mark Drela of MIT. By varying the wing twist across the wingspan, it was possible to achieve a span efficiency factor of 0.93 for the clean planform. Maximum washout (negative airfoil twist) is present at the wingtip and is equal to 2.6 degrees. Some of the results of the code, and the resultant wing lift distribution can both be seen in Figure 8.

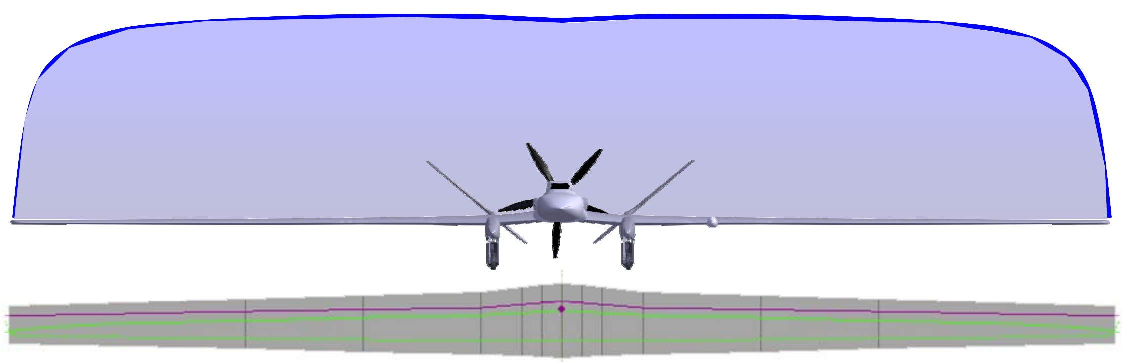

Figure 8 – XLFR5 Results

The airfoil polar shows the same operating point for both the cruise and takeoff conditions because *Adamant* is a "one-C_L airplane". Because *Adamant* is designed to fly at its best L/D C_L value and angle of attack throughout its mission in order to maximize efficiency, the wing is installed at that angle of incidence relative to the fuselage. With its quadricycle landing gear configuration, *Adamant* takes off without rotation, and with the fuselage being horizontal on the ground, cruise C_L must be used for takeoff.

No-rotation takeoff is not a large concern owing to high installed thrust and relatively low wing loading, which also allows for a clean wing configuration with no high-lift system. Another benefit of such a takeoff is obtained in the increased ground clearance that is allowed to the rear-mounted propeller. Observing other similar existing aircraft (primarily the *Predator*/*Mariner* UAV family), it can be seen that these aircraft also do not rotate on takeoff, primarily for the reasons of propeller clearance.

7. Performance

Drag calculations were made using a conventional drag method, taking into account the surface flow characteristics an Reynolds numbers of the components. The drag breakdown for the 45,000 ft loiter point can be seen in Figure 9. Methods from Schaufele [5] were used.

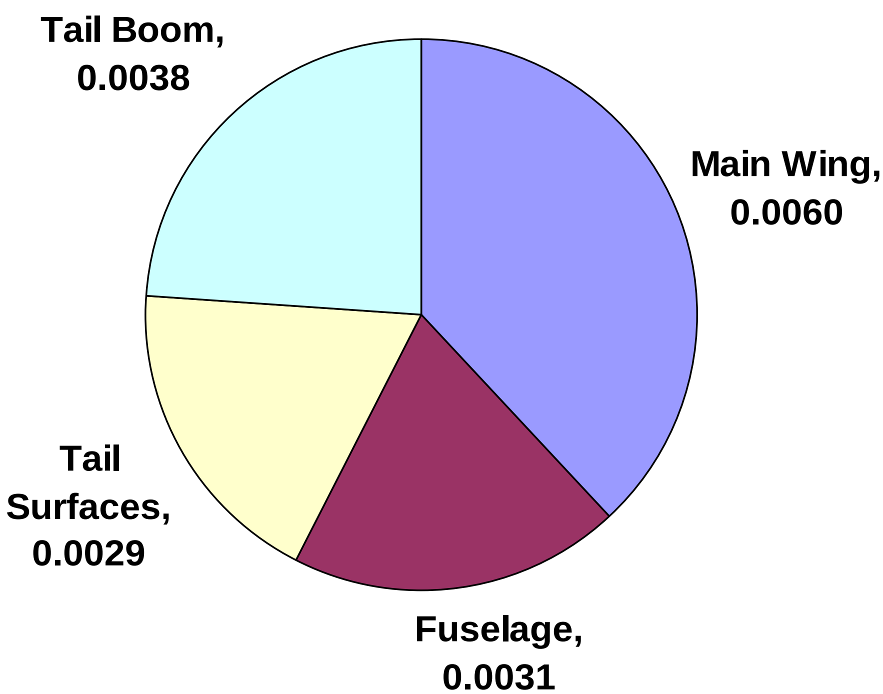

Figure 9 – Aircraft Drag Breakdown

Aircraft performance characteristics were calculated using the sizing code for a variety of relevant flight conditions. The thrust-to-weight relationship can be seen in Figure 10, which shows that the aircraft has positive thrust margins at the speeds and altitudes specified in the mission requirements. It can be seen that the aircraft can comfortably meet 200kts dash speed, although having to fly slightly faster than the best L/D speed of 180kts, as would be expected.

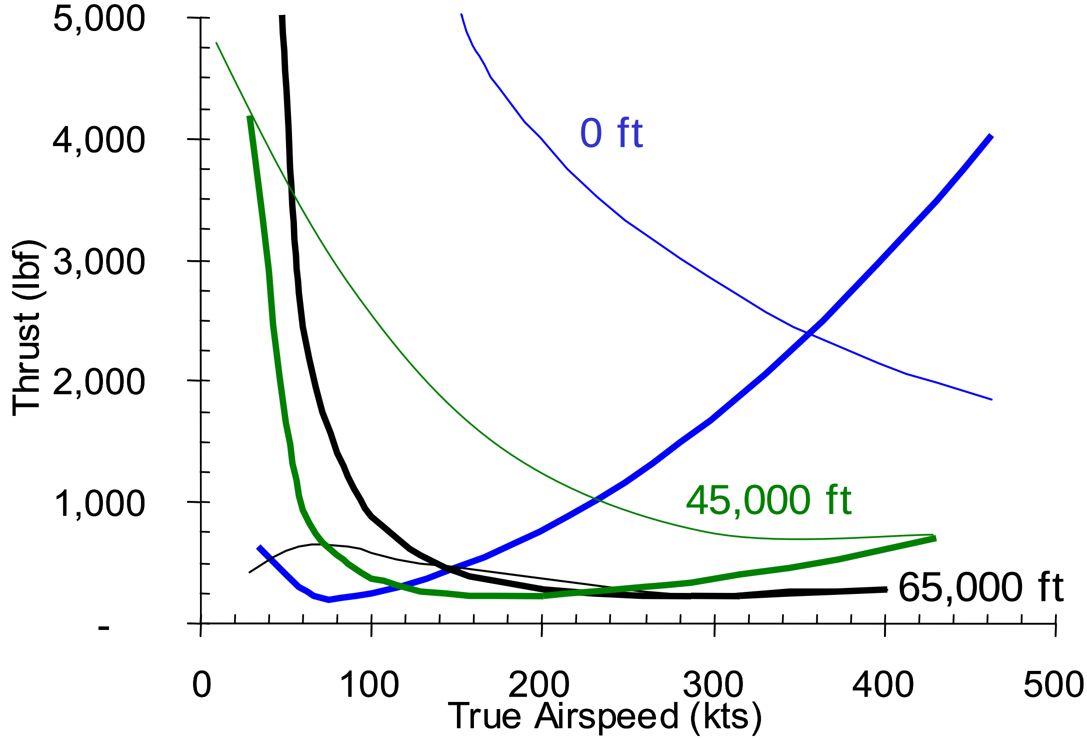

Figure 10 – Thrust vs. Drag Plot

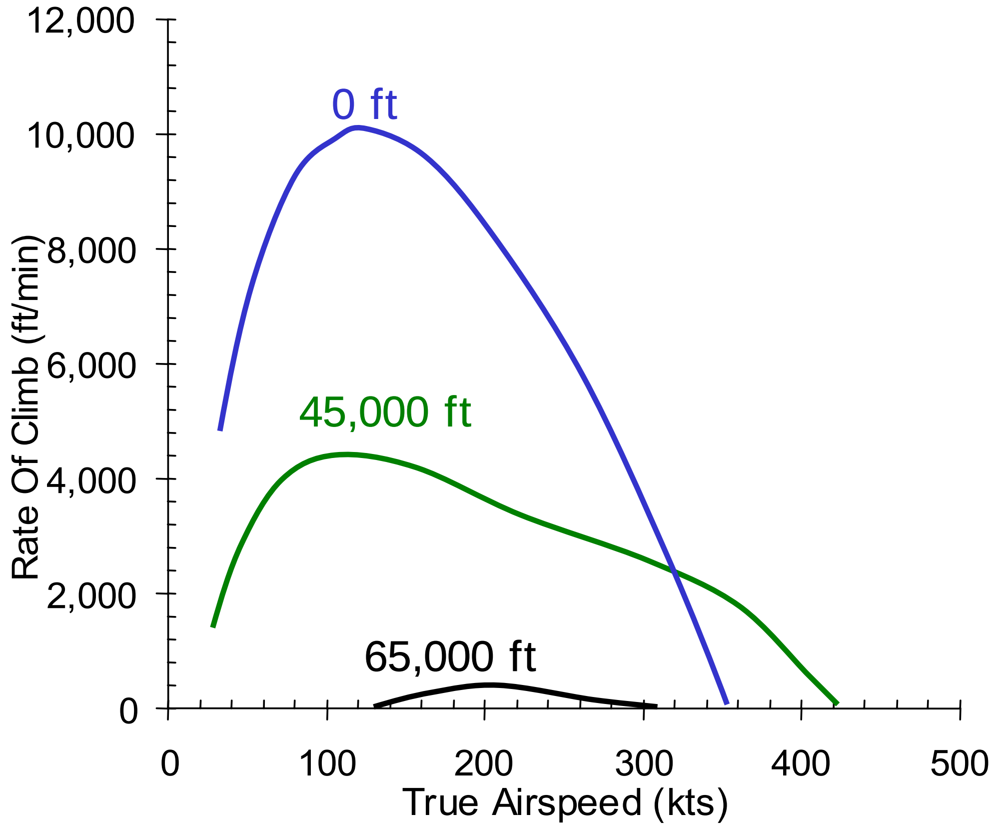

Figure 11 – Climb Rates

As previously mentioned, *Adamant* does not require rotation in order to meet the 5,500 ft takeoff constraint specified in the RFP. The aircraft has a balanced takeoff field length of 2,050 feet and a landing field length of 3,000 ft over a 50-foot obstacle. Takeoff and landing flightpaths are shown in Figure 12.

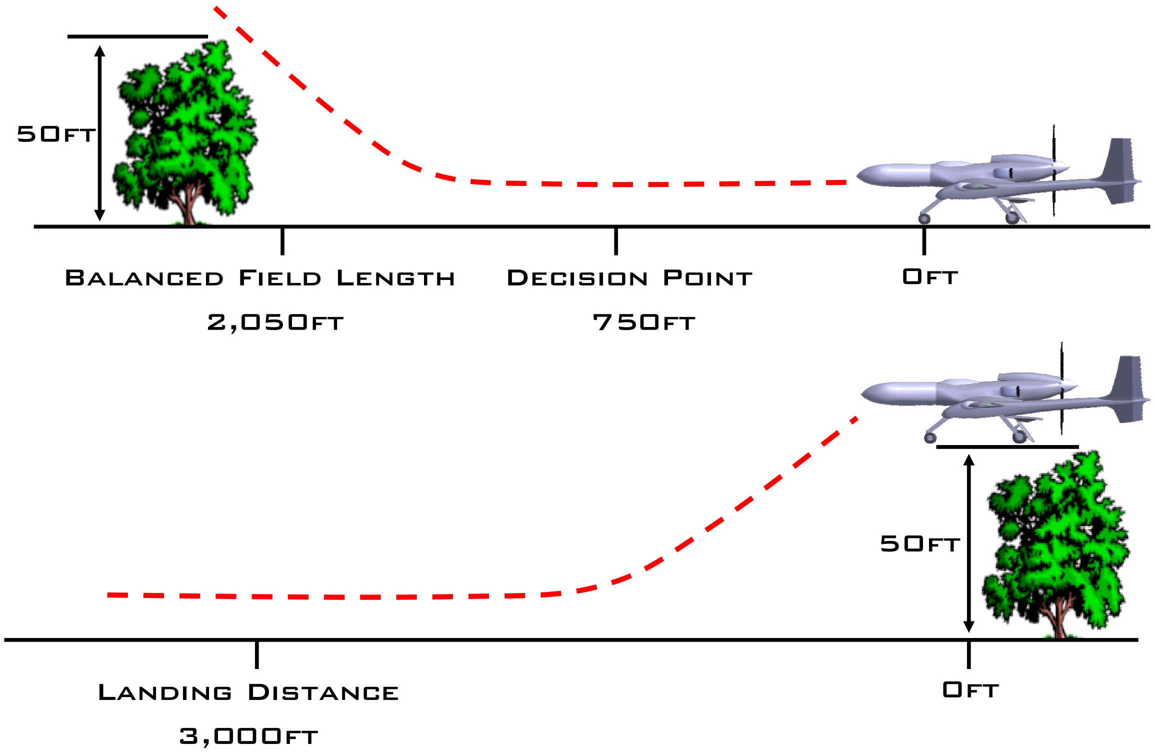

Figure 12 – Takeoff and Landing Diagrams

With current civilian airspace UAV regulations, *Adamant* cannot perform the climb to cruise altitude while in civilian airspace. The aircraft has to climb in a spiral flight path while remaining in segregated airspace, and only when above the majority of traffic can it proceed with the cruise segment of the mission. Because of this operational constraint, there is no distance credit taken for the climb portions of the mission when it is simulated using the sizing/analysis code.

8. Propulsion

Having established a required installed power value during initial aircraft sizing, a search of available turboprop engines in that power range was conducted. A number of appropriate choices were evaluated; however one engine in particular looked very attractive. The Rolls-Royce CTP800 turboshaft core was developed for the RAH-66 *Comanche* helicopter program. It is a modern engine, incorporating the latest in manufacturing, materials, and electronic control technology. A turboprop -4T modification of the base turboshaft engine was developed specifically for the Ayres LM200 regional cargo aircraft program.

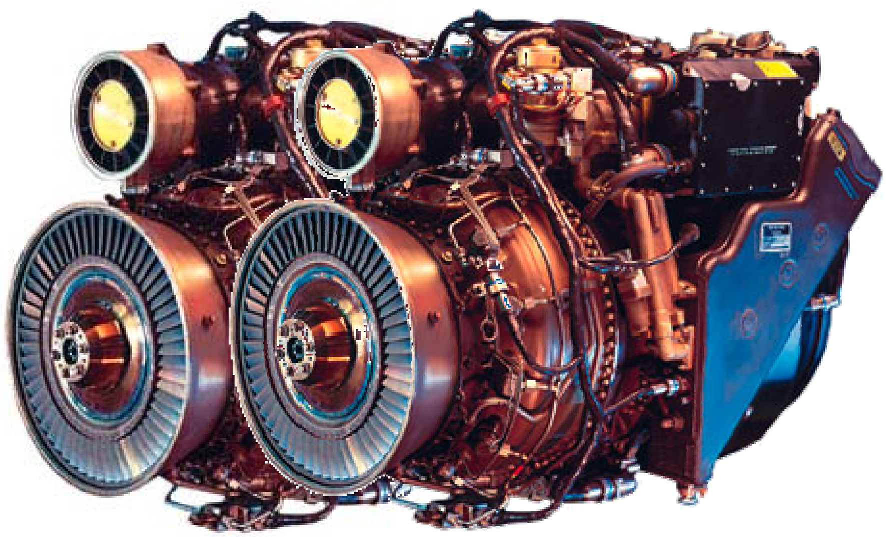

Figure 13 – Rolls Royce CTP800-4T

The most attractive feature of the Rolls-Royce CTP800-4T, aside from it having the optimum power rating for installation in *Adamant*, is the engine's "twin barrel" configuration. This engine layout joins two separate gas generators with a common gearbox allowing the combination of the best features of twin-engine and single-propeller aircraft.

Because each of the two combined turboshaft sections use individually redundant fuel and control systems, they can operate separately, and thereby act to significantly increase the safety and survivability of *Adamant*. With both of the engines driving a single propeller, the aircraft does not exhibit any detrimental effects during OEI operation. *Adamant* is fundamentally different in this respect from conventional twin-engine twin-propeller aircraft which are susceptible to drastically degraded controllability characteristics during OEI operation. Other benefits inherent in this engine choice are the lack of need for a ram-air turbine, distributed electric generation, and the ability to cross-start a flamed-out engine in flight.

Two possible choices for the engine installation exist – the initial "straight-through" installation is shown in Figure 14.

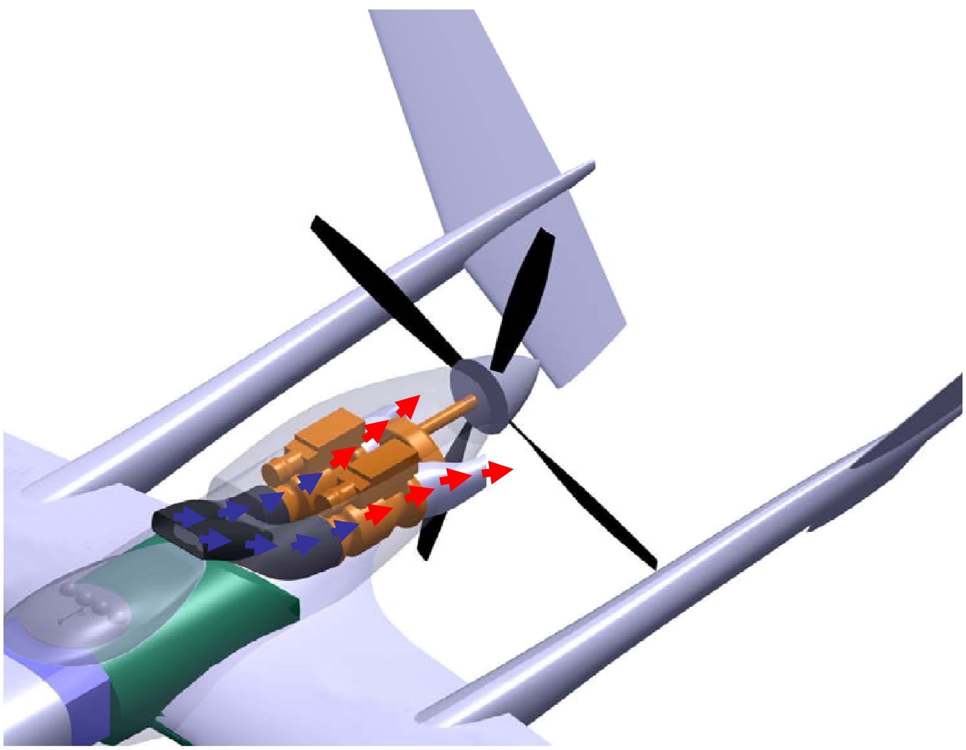

Figure 14 – Straight-through Engine Installation

This installation is ideal in terms of intake pressure recovery and extraction of excess thrust from the engine exhaust. However, the RFP specifically requires that an existing propulsion system be used on this aircraft design. This requirement is easily understood, when considering the 10-aircraft buy that the RFP mentions. Although the gas generator and the gearbox mechanical components have been developed, this type of installation would require the "swap" of the gearbox section from the front (intake) side to the rear (exhaust) side. Simpler than a full engine design, this type of a change was still considered to be too complicated for such a small aircraft buy, and an alternative had to be found.

The alternate engine installation choice is the reverse engine installation. This type of an engine installation can be seen in action in thousands of Pratt & Whitney PT6 engines currently flying in aircraft all over the world. The details of a typical PT6 tractor engine can be seen in Figure 15.

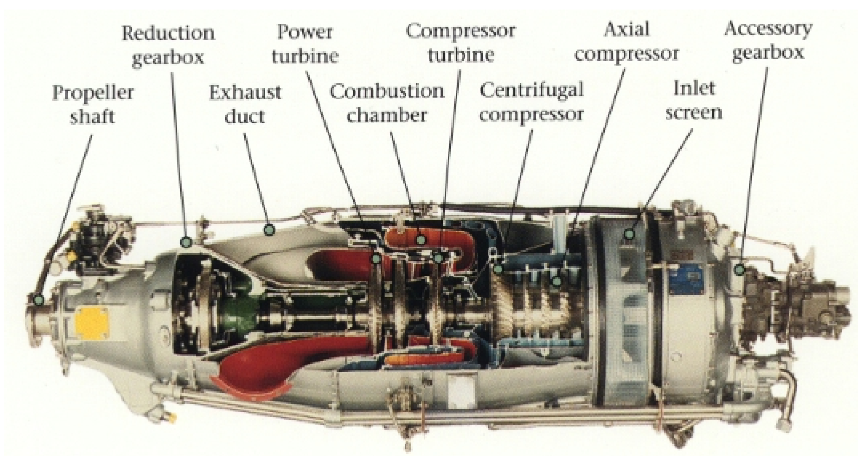

Figure 15 – PT6 Reverse Flow Turboprop Engine

Although the engine installation does not look as "clean" as the straight-through one, suffering from pressure recovery loss in the baffle intake and in the U-turn exhaust ducts, it offers a number of benefits. It is more compact and allows use of an off-the-shelf engine. An additional benefit present in this installation is the easy integration of a ballistic FOD separator, which will be very useful when flying through hail or in icing conditions. When considering the low indicated flight speed of *Adamant*, which can not contribute greatly to intake compression and the very low amounts of thrust present in turboprop engine exhaust, the benefits offered by the installation greatly outweigh its faults. Because of this, the final configuration of *Adamant* uses the reverse engine installation, shown in Figure 16.

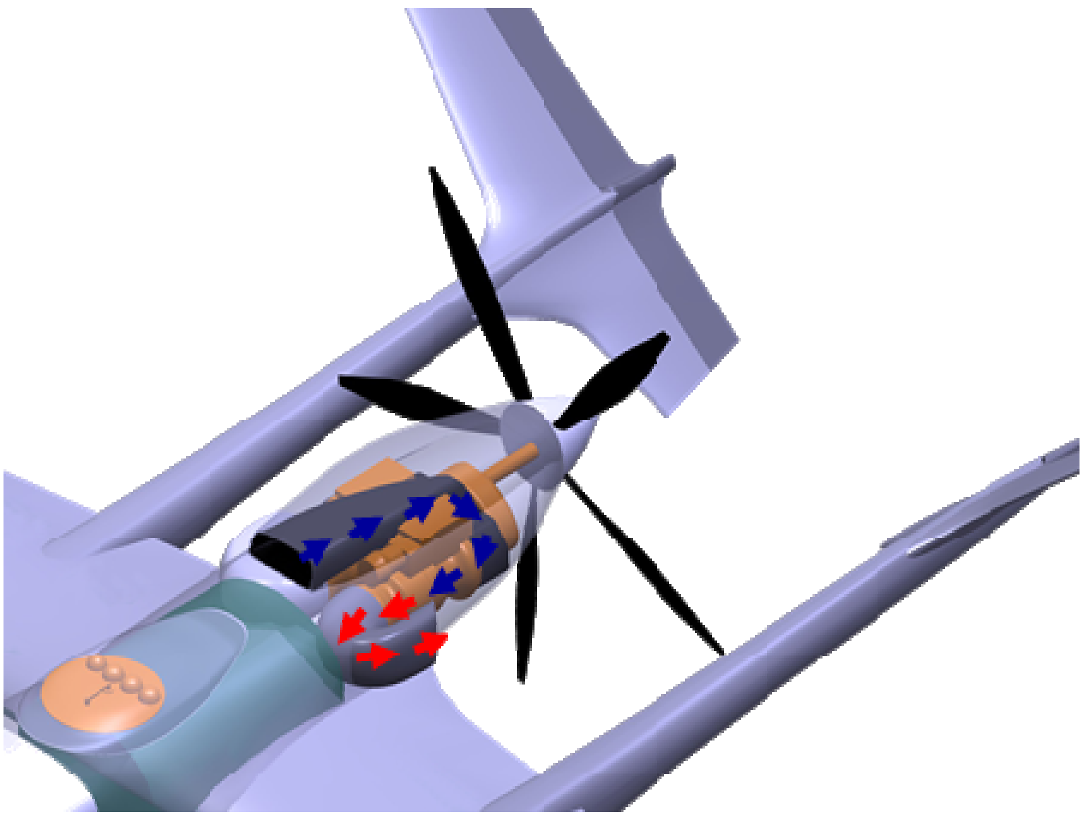

Figure 16 – Reverse Flow Engine Installation

Because no precise performance data could be obtained from Rolls Royce for the CTP-800 engine, a map for the T56 turboprop engine was modified both in overall SFC to account for the higher technology of this newer engine and in altitude thrust lapse to account for its higher compression ratio. As allowed by the RFP, the engine map was also extended by extrapolation to produce engine performance values at altitudes up to 65,000 ft MSL. The engine map used in the sizing code is attached in Appendix 1.

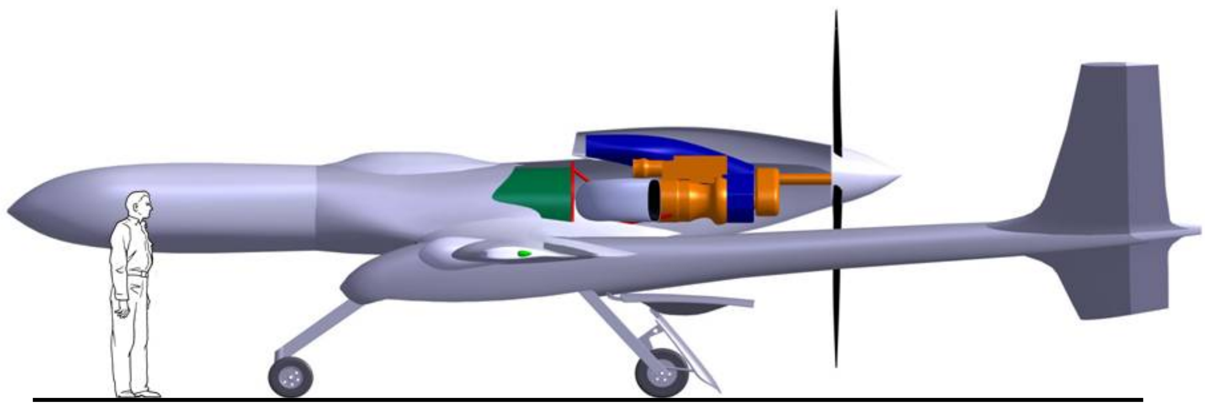

Figure 17 – CTP800-4T Engine Installation

The Rolls-Royce CTP800-4T installation can be seen in Figure 17. The installation is accomplished in a relatively conventional way – with the engine being attached to the rear spar/bulkhead with a metal tube-and-truss mount. Because of its location in the aircraft, the engine is easily accessible by ground crew for service or replacement. Although being located slightly above shoulder-level position of a maintainer, the engine is still easily accessible from the ground using a small step-up.

9. Propeller Sizing

In the history of propeller-powered high-altitude aircraft, propeller/gearbox oftentimes became the most troublesome area of design and development. Owing to the large air density changes encountered within the range of aircraft operating altitudes, the aircraft is likely to suffer from degraded propeller performance in at least one of the mission flight conditions. When designing the propeller to be used on *Adamant*, the middle range (55,000ft) of high altitude loiter was established as the sizing point for which to optimize the propeller performance. The software JavaProp[6] was used in the design of the propeller. This software, which is based on blade element theory is considered quite accurate for simple propellers with low power loading. The performance results for the *Adamant* propeller at the 55,000ft loiter point can be seen in Figure 18.

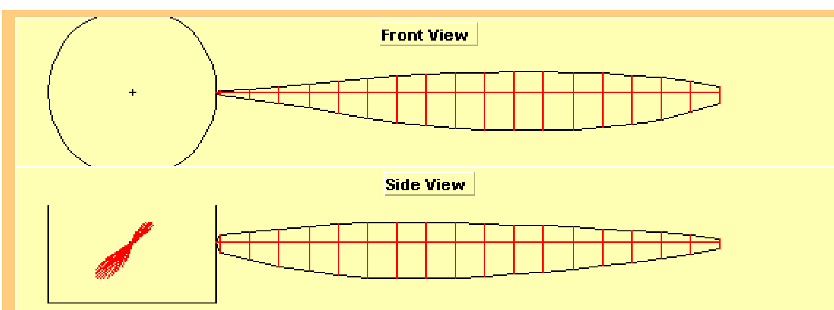

v/(nD)	1.429
Efficiency η	90.88 %
Thrust T	9.9 N
Power P	1.09 kW
β at 75%R	34.2479°
v/(ΩR)	0.455
loading	low
Ct	0.0011
Cp	0.0018
Pitch H	5.61 m

Figure 18 – Propeller Sizing Output

In order to ensure efficient operations at both loiter points, the constant-speed propeller will modify the collective blade angle-of-attack according to values in Table 3. Propeller pitch will be increased to allow efficient flight in less dense air at 65,000 ft and reduced to allow for flight in denser air at 45,000 ft. Although blade twist distribution obviously remains the same, propeller efficiencies remain in the 90% range at both the

45,000ft and the 65,000ft loiter altitudes. The propeller efficiency degrades dramatically at sea level, however the aircraft spends very little time at that low altitude, and has high available power at that point. It must be noted that propeller operation was estimated at a propeller speed of 1,200 revolutions per minute, which is the standard output speed for the CTP800-4T engine gearbox. An add-on multi-speed gearbox would be advantageous to allow for efficient operation at all altitudes, but was prohibited by both the RFP existent propulsion system limitation and cost considerations for aircraft development.

Table 3 – Propeller Performance

Altitude (ft)	Treq'd (lbf)	Δ Pitch (deg.)
45,000	300	-4 °
65,000	225	+8 °

Dynamic disturbance will likely be created by the propeller tips passing close by the tailbooms of the aircraft. With the propeller tip Mach numbers reaching 0.75, there is considerable possibility of control, resonance and structural problems being created in the tailbooms on by this interference. Because it is not feasible to conduct a detailed evaluation of this issue at the current point in the design, an attempt was made to instead mitigate it by providing a clearance equal to that seen in existing real-world aircraft. With the Cessna C-337/O-2 *Skymaster* propeller installation acting as a guideline, the propeller-tip to boom clearance of 6 inches was implemented on *Adamant*.

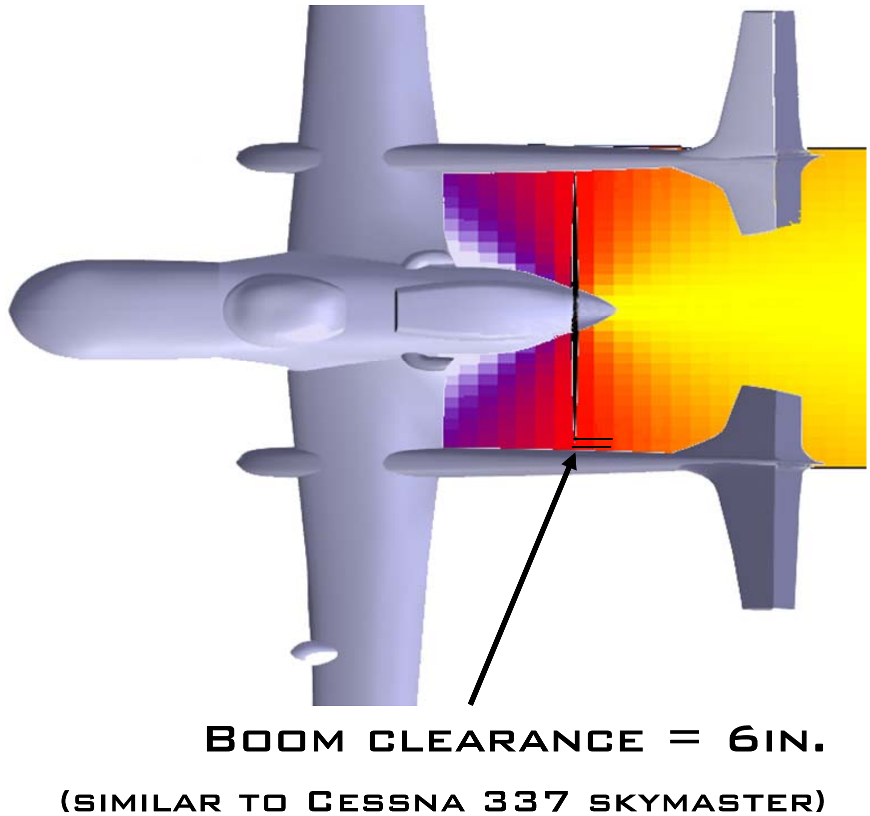

Figure 19 – Propeller-to-Boom Clearance

According to the requirements of the RFP, a total of 1500 watts (approximately 2HP) of electrical power must be supplied to the on-board systems. Therefore, some engine power must be dedicated to running electric generators. However, environmental systems for the payload compartment, such as heating and air conditioning must also be supplied with power, and the inherent inefficiencies in the system must be accounted for. Assuming a 5HP total load, and a generator efficiency of 50%, 10HP of engine power needs to be diverted for electricity generation. In simulation of aircraft performance, engine shaft power output was reduced by this amount to account for electric power generation.

10. Weight and Balance

The aircraft weight breakdown is presented in Table 4. All of the weights were estimated using equations from Roskam[7]

Table 4 – Aircraft Weight Breakdown

Item	Weight (lbs)	Station (in)
Fuselage	326	160
Main Wing	508	147
Landing Gear	197	148
Engine	1,197	229
Engine Installation	390	215
Vertical 1	63	360
Vertical 2	63	360
Fuel System	373	150
Engine Start	29	225
Avionics	525	113
Tailbooms	285	200
Fuel Dump	20	170
Flight Controls	331	147
Air Induction	123	210
Electric System	264	147
Mission Payload	852	61
Fuel	4,800	162
Weight Empty	**5,546**	**lbs**
Takeoff Gross	**10,346**	**lbs**
Quarter Chord	**158**	**in**
Rear Limit	**171**	**in**

The CG excursion of the aircraft can be seen in Figure 20. It can be seen that owing to the on-CG location of the fuel tanks, the aircraft center of gravity moves very little during flight, and remains within controllability margins of the airframe. The deployment of the 68 lbs of dropsondes does not significantly move the CG location, with the total CG travel during the mission being limited to approximately 6% MAC.

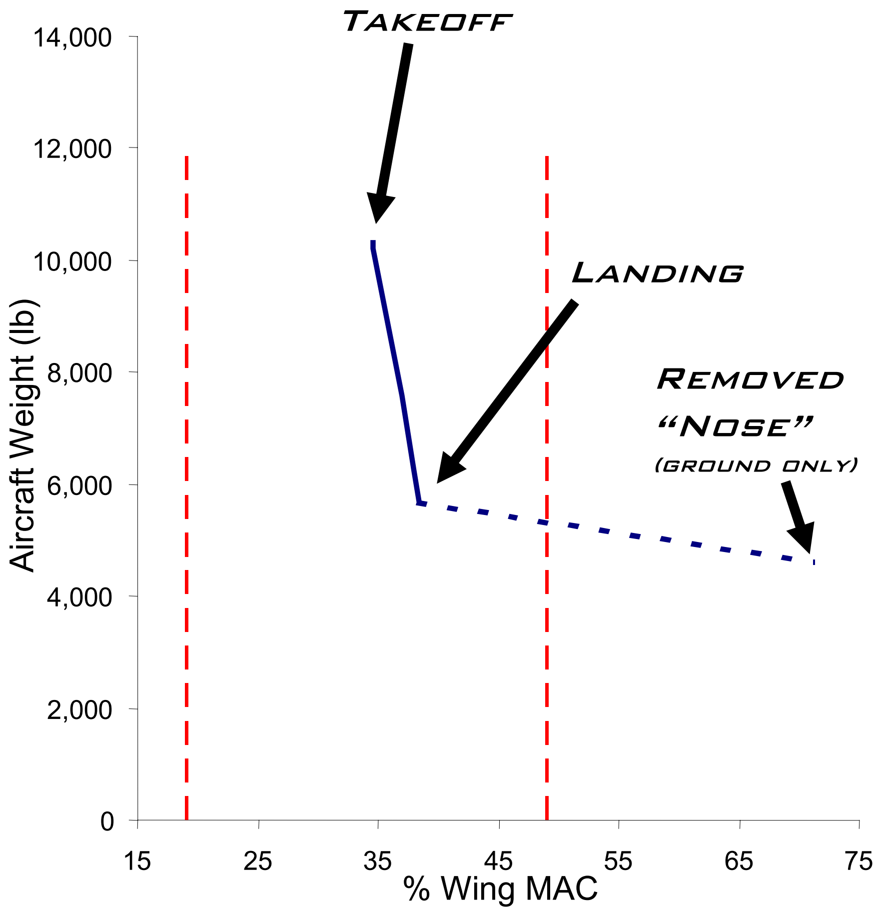

Figure 20 – Aircraft CG Excursion

The aft limit was determined using the AVL code, coinciding with the neutral point of the airframe. The forward limit is also determined using the AVL software, using the conservative 10° elevator deflection at loiter condition. Using these calculations, the 30% MAC allowable CG range shown in dashed red lines in Figure 20 was obtained. Although the aircraft CG exceeds this range with the nose section and the payload contained inside removed from the aircraft, the aircraft remains statically stable on the ground, and it is obviously not intended to be flown in such a configuration.

11. Stability and Control

The controls configuration of *Adamant* is quite conventional, being comprised of two movable surfaces on the V-tails and two ailerons on the main wings. All of the controls use electro-hydraulic actuators located near the aerodynamic surface. This not only reduces the maintenance requirements of the aircraft, but entirely eliminates hydraulic systems in this aircraft. The control surface layout can be seen in Figure 21.

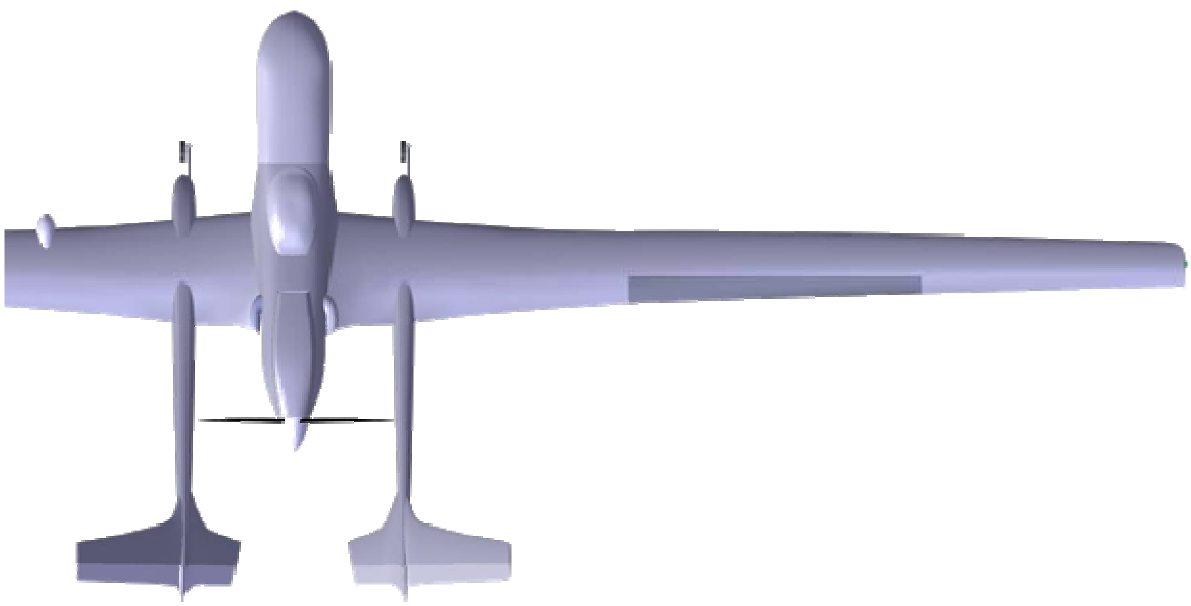

Figure 21 – Control Surfaces

Although the ailerons would be capable of generating a maximum rolling moment if they were to be installed as far outboard as possible, it was chosen to install them mid-span on the wing to avoid control reversal. Ailerons installed on high-aspect ratio wings tend to cause the wing to twist, modifying the overall angle-of-attack of the outboard portion of the wing to such an extent that the resultant force generated by the wing is in the opposite direction from that commanded by the control input. Specific sizing to avoid these issues is difficult to undertake at this stage of the design; however, judging that the aircraft does not have a requirement for a high roll rate, and thus high aileron authority, this installation was considered to be beneficial.

An initial tail volume sizing procedure for *Adamant* was carried out using values obtained from existing aircraft in the same category. The V-tails on *Adamant* and other aircraft were converted to their horizontal and vertical equivalents using equations below.

$$\mathbf{S_{HT}=S_{TS}*cos(\theta)^2}$$

$$\mathbf{S_{VT}=S_{TS}*sin(\theta)^2}$$

This method is considered more accurate than using direct projections of the V-tail surface. The values used on *Adamant* compared to the values used on the other aircraft can be seen in Figure 22.

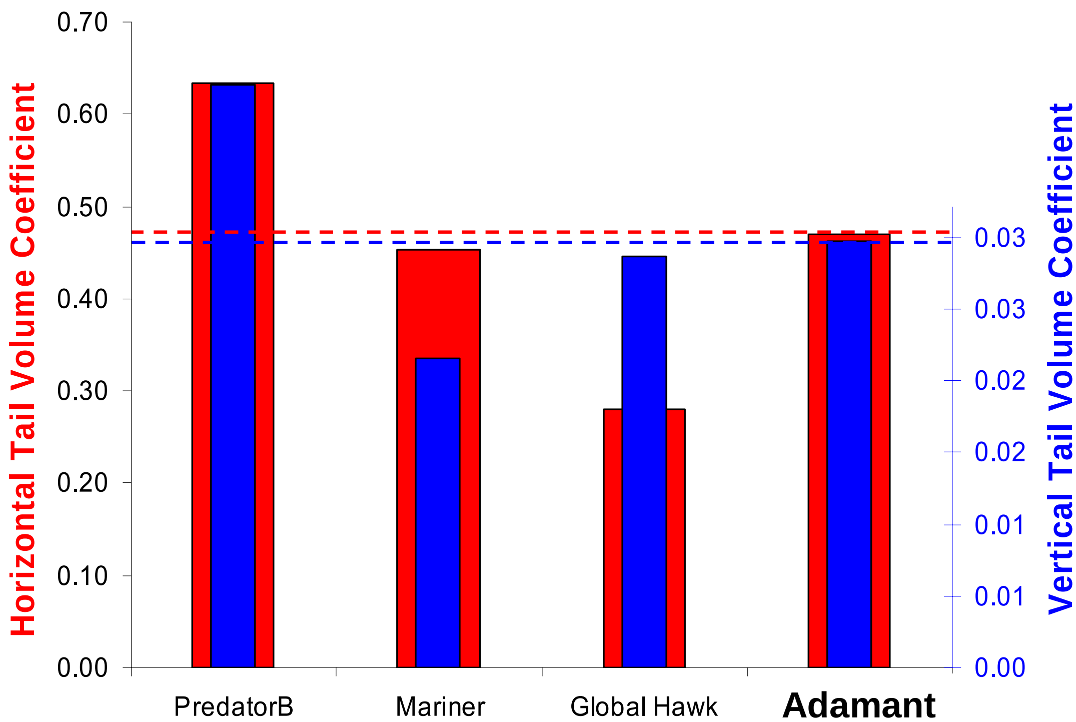

Figure 22 – Control Volume Coefficients

The configuration was evaluated using the AVL (Athena Vortex Lattice) code, a piece of software created by Mark Drela of MIT. Using an extended vortex-lattice model, the software uses input aircraft geometry to conduct trim and dynamic stability analysis. The aircraft geometry that was input into AVL to analyze the *Adamant* configuration can be seen in Figure 23. The input file used in AVL analysis is included in Appendix 2.

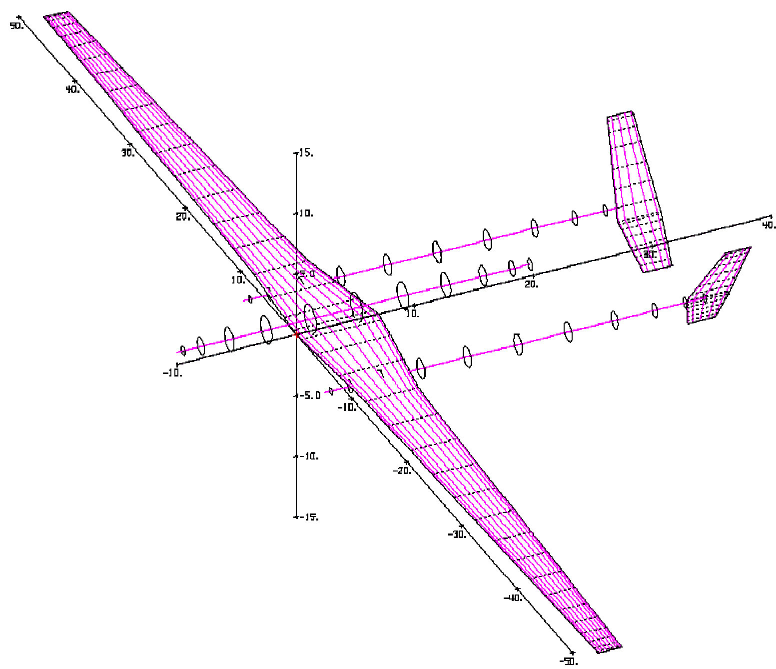

Figure 23 – Geometry for AVL Analysis

All of the aerodynamic surfaces, the control surfaces, and the major bodies of the configuration were modeled in AVL. The surfaces are modeled by single-layer vortex sheets, discretized into horseshoe vortex filaments with the trailing legs of those filaments going intro the freestream direction. In their turn, slender bodies are modeled by source+doublet filaments. The control derivatives for the aircraft, obtained at a CG position representing a rear-limit flight condition, can be seen in Table 5.

Table 5 – *Adamant* Control Derivatives

	Angle of Attack	Angle of Sideslip	
z force	CL_{α} = 6.039737		
y force		CY_{β} = -0.438214	
roll x mom.		Cl_{β} = -0.022467	
pitch y moment	Cm_{α} = -0.005149		
yaw z moment		Cn_{β} = 0.110688	

	Roll Rate p	Pitch Rate q	Yaw Rate r
z force		CLq = 6.516037	
y force	CY_{p} = 0.050134		CYr = 0.23001
roll x moment	Cl_{p} = -0.630488		Clr = 0.244945
pitch y moment		Cmq = -12.456394	
yaw z moment	Cn_{p} = -0.106601		Cnr = -0.073412

	Aileron δ1	Elevator δ2	Rudder δ3
z force		$CL_{\delta 2}$ = 0.004533	
y force	$CY_{\delta 1}$ = 0.000294		$CY_{\delta 3}$ = 0.00576
roll x moment	$Cl_{\delta 1}$ = -0.012307		$Cl_{\delta 3}$ = 0.000069
pitch y moment		$Cm_{\delta 2}$ = -0.023169	
yaw z moment	$Cn_{\delta 1}$ = 0.000004		$Cn_{\delta 3}$ = -0.00169
Trefftz drag		$CDff_{\delta 2}$ = 0.000190	

From these derivatives it can be concluded that the aircraft is controllable and statically stable in all body-reference axis. Detailed modeling of the aircraft control system performance and control surface effectiveness must be conducted in higher detail during the latter stages of design development.

12. Structures and Materials

Adamant is designed to be primarily manufactured from composite materials. Owing to their high strength-to-weight ratio, ease of manufacture and relatively low amount of preparation required to manufacture high-quality surface finish parts, composites seemed to be an ideal material to use in manufacture of *Adamant*. The structural arrangement of the aircraft is quite conventional and can be seen in detail in Figure 24.

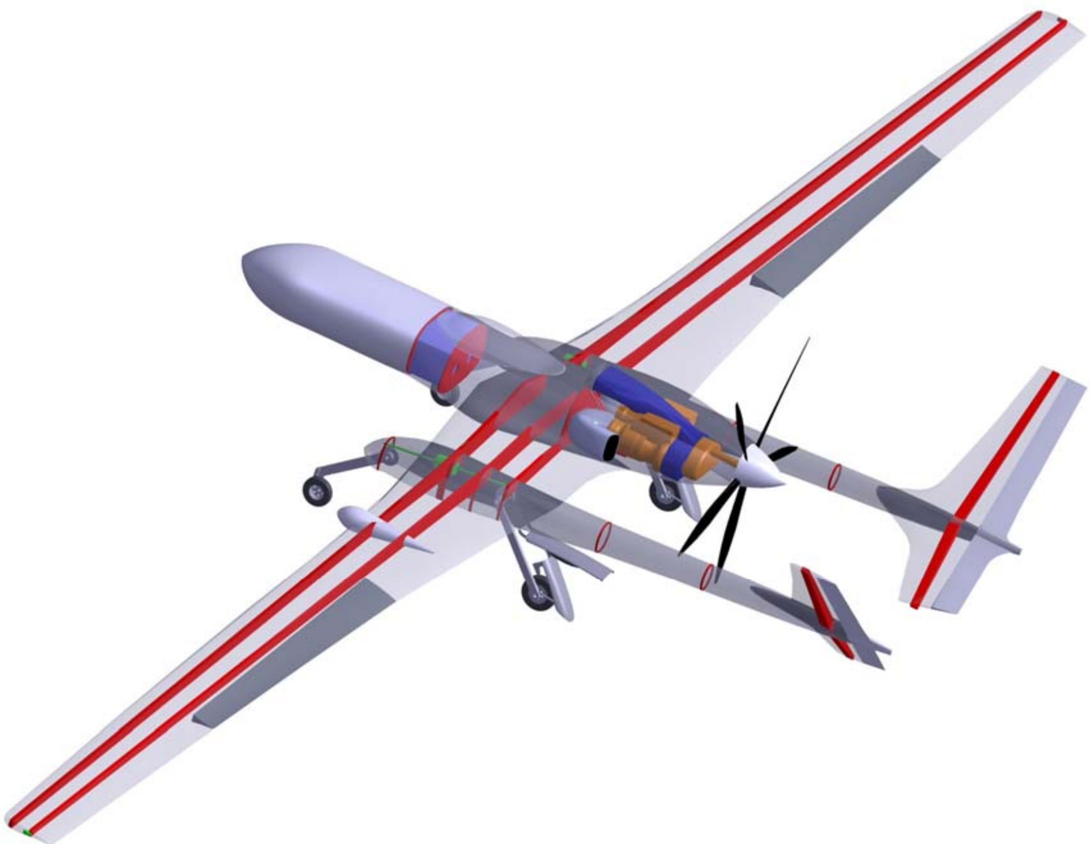

Figure 24 – Aircraft Structural Configuration

Two main spar shear webs run down the entire length of the wing, carrying the bulk of the aerodynamic bending and torsional loads, while a shorter supplementary spar connects the tail-booms, and the engine firewall/mount. Much of the load is carried in carbon-fiber spar caps located in the wing top skin. The V-tails have a single spar running through the span of the surface, and a number of ribs are located spaced throughout the fuselage and the tailbooms. It is likely that the torsional loads carried through the tailbooms will be lessened by virtue of the relatively symmetric disposition of force-generating aerodynamic surfaces above and below the boom axis. This may allow for the boom structure to be optimized for bending loads, as opposed for both bending and torsion.

The material distribution in the aircraft can be seen in Figure 25. Most of the aircraft is made form a variety of composite materials, with metals being used in locations requiring ballistic or heat protection. The structural components of the airframe are manufactured from carbon fiber, with the control surfaces being made from Kevlar®. Owing to its removable configuration, the nose section can be custom-manufactured – in the current iteration it is made from fiberglass in order to allow radio transparency for the mission data-gathering equipment contained within. However, some Kevlar® use is sure to be warranted, considering that the nose section is a very likely location for bird strikes and other FOD (Foreign Object Damage).

The aircraft skins will be composed of carbon fiber, which can be seen to comprise the major structural component of the aircraft. A copper mesh will be embedded in this skin in order to mitigate the effects of lightning strikes.

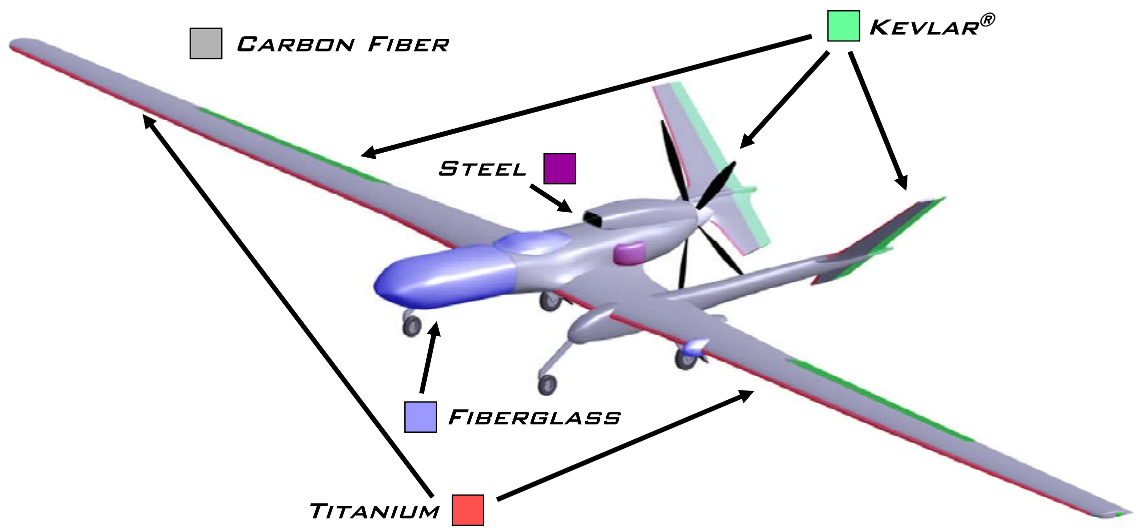

Figure 25 – Materials Usage

An important concern with the RFP requirements was the specified G-load requirement, which is set at +9/-6G ultimate. Obviously, the intent of the RFP originators was to making sure that the aircraft is structurally secure during the flight in the disturbed ambient conditions that exist inside a hurricane wall. However, during spar sizing it became obvious that a high-aspect ratio wing such as that of *Adamant* will suffer a tremendous weight increase when being designed to such a high ultimate G load. A piece of information that seemed to not fit with the requirement of the RFP was the fact that the current mission of the 53rd Weather Reconnaissance Squadron is performed by conventional C-130 aircraft. Upon further investigation, it was found out that the ultimate load of the C-130A aircraft at full fuel, empty payload is only 3.5 Gs. This does not present an issue since during the mission, the aircraft does not penetrate the hurricane head-on, but instead "crabs" into the wind, never seeing sharp changes in perceived wind speed. This approach is very safe, and the 53rd has flown over 100,000 mishap-free hours.

The RFP G-load requirement was kept in mind as detailed spar sizing was proceeded with. Using a code developed in Microsoft Excel, it was possible to use simple bending theory to optimize a spar lay-up for a stress condition occurring at a given G-load. This tool was used to both size the spar and to evaluate in detail the weight effects of differing G-load requirements. A spar cap lay-up sized for 4Gs can be seen in Figure 26 below.

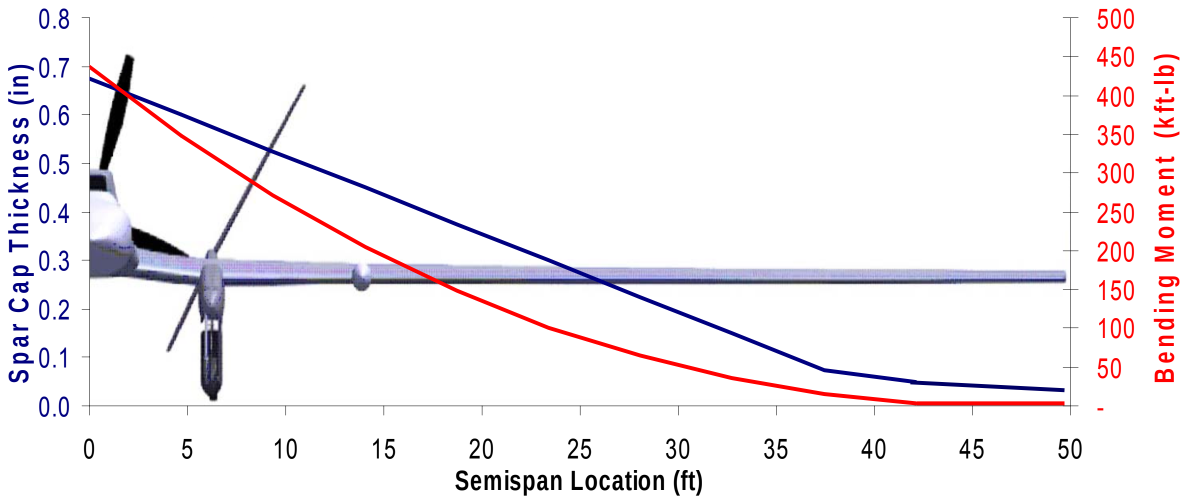

Figure 26 – Wing Spar Lay-up

The bending moment, shown in red can be seen to change in a parabolic manner, while the spar cap lay-up thickness decreases linearly for most of the wing semi span. This is caused by the variable chord of the spar cap, which is 12 in at the wing root and 3 in at the tip. Using the material properties of unidirectional carbon-fiber composite, the all-up weight of the 4-G spar cap lay-up was determined to be approximately 322 lbs, which was well below the weight predicted by the wing weight equations used in mission simulation/aircraft sizing. This same code output a weight of 876 lb for a spar sized for a 9G ultimate loading, which corresponds to an increase in spar weight of more than 250% compared to the 4G condition.

Upon evaluation of the V-n diagram of *Adamant*, shown in Figure 27, it can be observed that the limit load on the aircraft goes no higher than +3.3/-1.65 Gs at loiter speed.

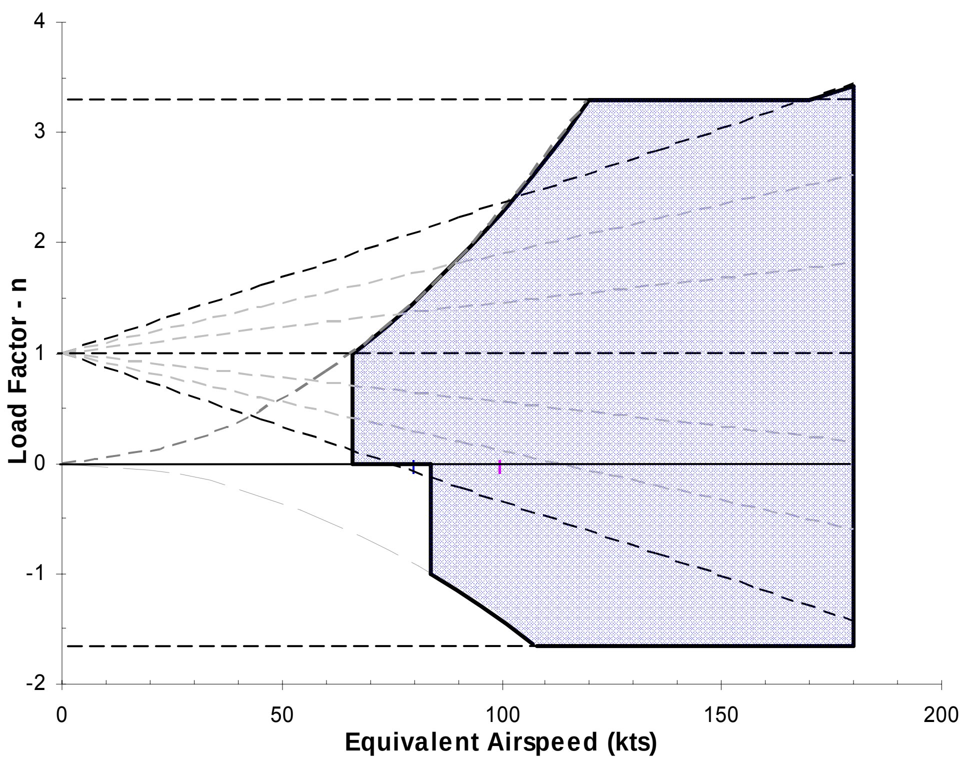

Figure 27 – V-n Diagram

Gust loads have a minor effect on the airframe structural considerations, increasing ultimate positive load to 3.43 at speeds approaching V_D. The V-n diagram shows that the aircraft is limit-loaded significantly lower than the +6/-4 G limit and +9/-6 G ultimate loads specified in the RFP. Adhering to the 9G ultimate load RFP constraint would drive the aircraft weight up dramatically, and result in a much larger, more expensive aircraft. The C-130 safely performs a hurricane-hunter mission with an ultimate G-loading of less than half of that specified in the RFP, while the V-n diagram states that the Adamant configuration has a limit load of approximately +3.3G. Based on these findings, it appeared that decreasing the RFP G-load requirement would result in a better and cheaper aircraft for the customer.

In order to pick the ultimate load value for *Adamant*, a safety factor had to be applied to the ultimate load calculated from the V-n diagram. Traditionally, the ultimate load is created by an application of a factor of safety of 1.5 to the limit load. This was defined in a 1930s Air Corps specification based upon the ratio between the ultimate tensile load and yield load of 24ST aluminum alloy.[8] Because modern design techniques, high-performance composite materials and application to an unmanned aircraft can allow a lower degree of safety, a safety factor of 1.2 and an ultimate load of +4 G were chosen to be used on *Adamant* during preliminary design.

13. Landing Gear

The quadricycle landing gear configuration used on *Adamant* has found use in a number of aircraft, with the Boeing B-52 being perhaps the most widely-known. However, the most similar aircraft installation is certainly that used on the Scaled Composites Model 318 *White Knight* airplane, pictured in Figure 28 with an underslung payload.

Figure 28 – White Knight Landing Gear Configuration

The landing gear of *Adamant* is configured very similarly to that of the *White Knight*, with the nose wheels being allowed to freely castor, and steering being accomplished by differential braking of the rear wheels. The landing gear configuration synergistically allows for a number of benefits to the overall mission, allowing for nose section removal, clear fuselage underbody and static stability on the ground. By using identical left/right landing gear sets, part commonality is increased, manufacturing is simplified and component servicing is made easier.

Because both the front and the rear landing gear legs have to travel through a retraction arc of approximately 135 degrees, retraction actuation using linear actuators was difficult, if not impossible to implement. However, the use of worm-gear actuators allowed to both use an electrical system to accomplish landing gear retraction, and to use a common motor to retract both the front and rear gear legs. The gear legs are spaced span-wise for clearance in retracted position, while the wheels share a common ground track. A detail of the landing gear installation can be seen in Foldout 2. The retraction geometry and component layout of the landing gear can be seen in Figure 29.

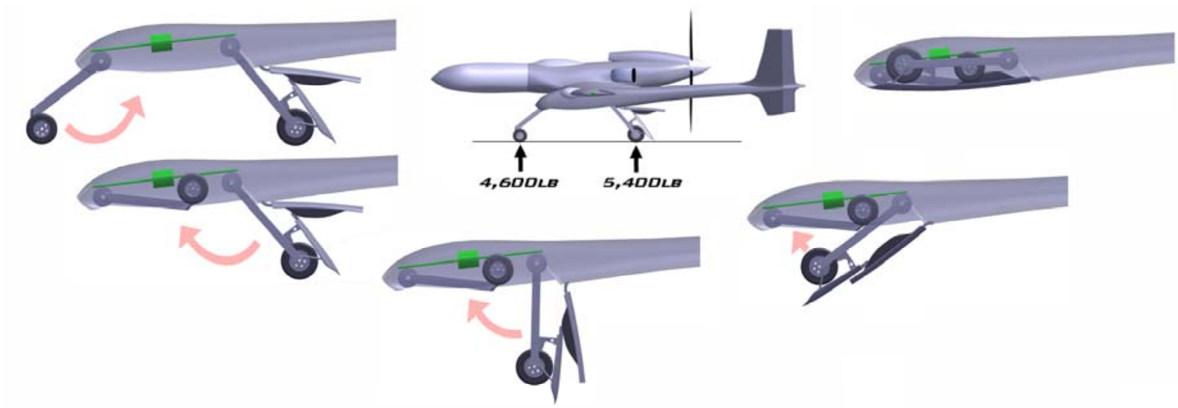

Figure 29 – Landing Gear Retraction Geometry

The landing gear actuator mechanism is coupled to the landing gear doors in order to have a secondary role of gear door actuation. This allows for a more rugged and simple landing gear arrangement, one that is likely to be lighter and cheaper. Although the gear door configuration creates significant drag when in the process of retraction, the aircraft possesses sufficient pitch authority to negate the resultant transient nose-down moment. A conventional side-retracting gear door configuration can be used as an alternative, if this configuration proves to be not sufficiently advantageous in the process of detailed design.

14. Fuel System

The aircraft fuel system is of a simple construction and is designed to keep the aircraft fuel load on the center of gravity. The fuel system is comprised of a main body tank connected to inboard fuel tanks, and two interconnected outer wing tanks. The major volume of the outer wing tank is located between the front and rear main wing spars, while a smaller tank section is located inboard of the aileron, between the rear main and the auxiliary spar. The fuel tanks are manufactured during wing cure and are gravity-fed to a fuel pump pickup located at the bottom of the main body fuel tank. A convenient refueling location exists in the port tailboom nose cone. With all tanks interconnected, the aircraft can be easily refueled from this “single-point” refueling location.

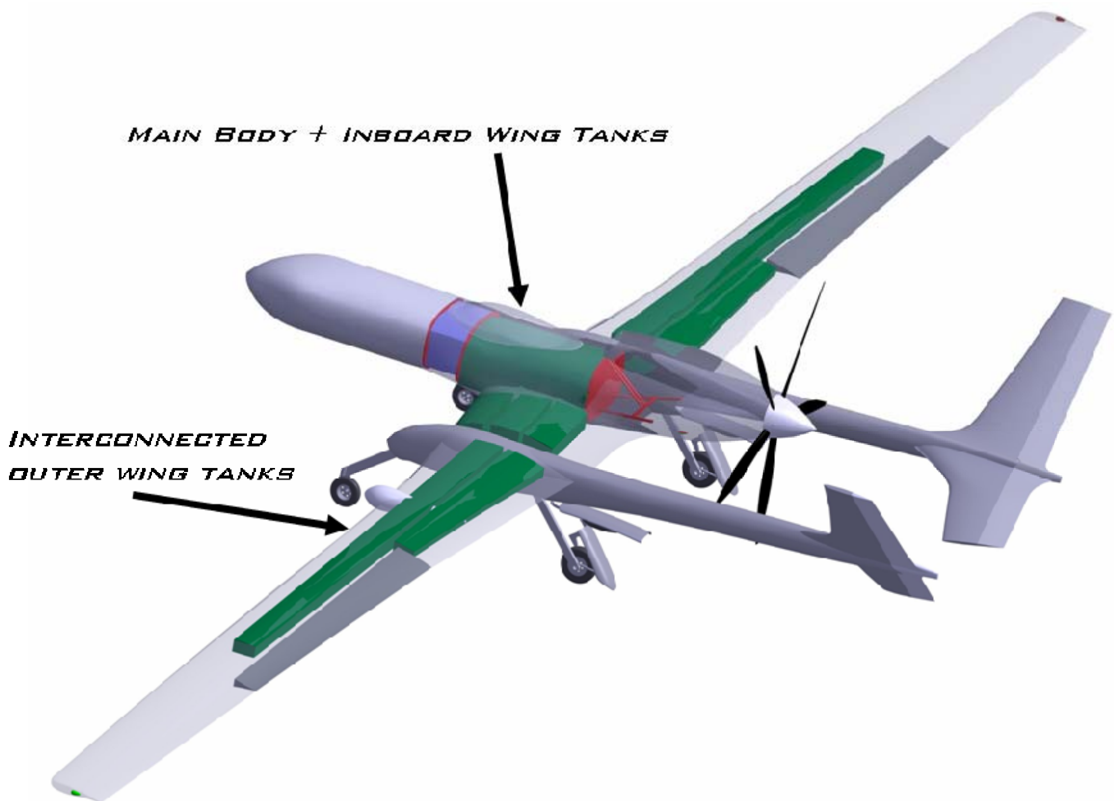

Figure 30 – Fuel Tank Configuration

Although the aircraft requires only approximately 100 ft^3 of fuel to complete its mission, the fuel tanks are sized with excess space, having the volume of 115 ft^3. This can be used for either over-gross weight operations or for ferry missions and fuel venting and pressurization purposes. In addition, in order to avoid fuel leakage out of the tanks in an over-fill or fuel surge situation, some of the fuel tank volume in the wingtips is dedicated to fuel surge tanks.

15. Alternate Missions and Payload Systems

Owing to its innovative design, *Adamant* is capable of performing a wide variety of missions other than the one specifically required by the RFP. A variety of payloads in the 800lb range can be installed in the nose section instead of the dropsondes/support equipment payload of the RFP mission. Different nose sections can be custom-made for payload having specific requirements, such as radio-transparency or shape. Because the nose section does not constitute a structural aircraft component, such a customization should not be difficult to design or manufacture.

Nose section change can be accomplished using a standard-size truck, allowing aircraft reconfiguration and servicing to be done quickly and easily. The landing gear configuration allows the aircraft to remain statically stable with the payload section on or off and with fuel tanks in an empty or full state. This procedure can be seen in Figure 31.

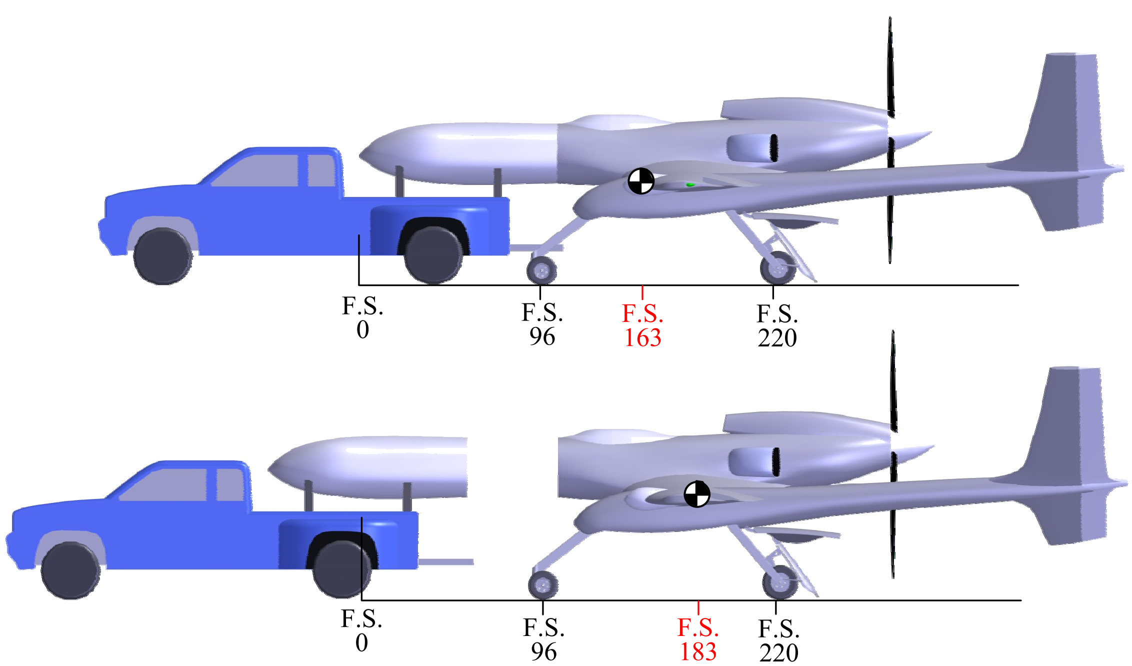

Figure 31 – Payload Section Removal

The modular nose concept can be leveraged even further by using it to achieve airframe aerodynamic customization. In case of a payload that is outsize either in weight or in length, the aircraft MAC location can be modified by an inclusion of a canard "trim" surface on the custom-made payload fairing, in a manner demonstrated in Figure 32. Such a nose section change will obviously require a more involved design process, when compared to a simple payload fairing modification mentioned earlier. Nonetheless, this capability is sure to be a very useful one, adding even more modularity and flexibility to the overall configuration.

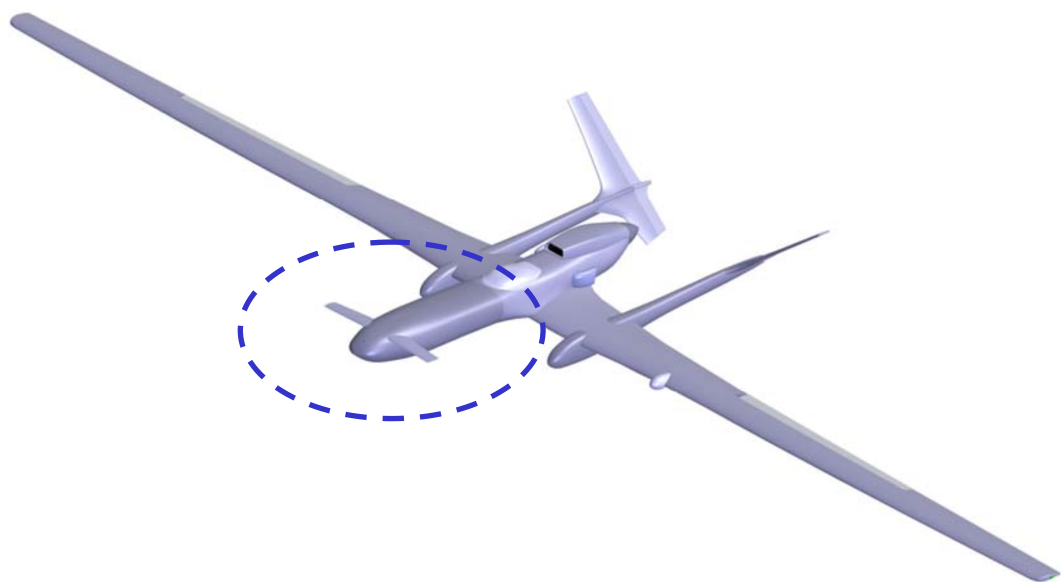

Figure 32 – Aerodynamic Payload Fairing Modification

The modularity of the removable nosecone contains a large number of advantages, but due to its off-CG location, no payloads located there can have a large-weight in-flight deployable component. Such payloads must instead be located on or near the CG of the aircraft. This can easily be done by suspending an aerodynamic fairing underneath the main fuselage as shown in Figure 33.

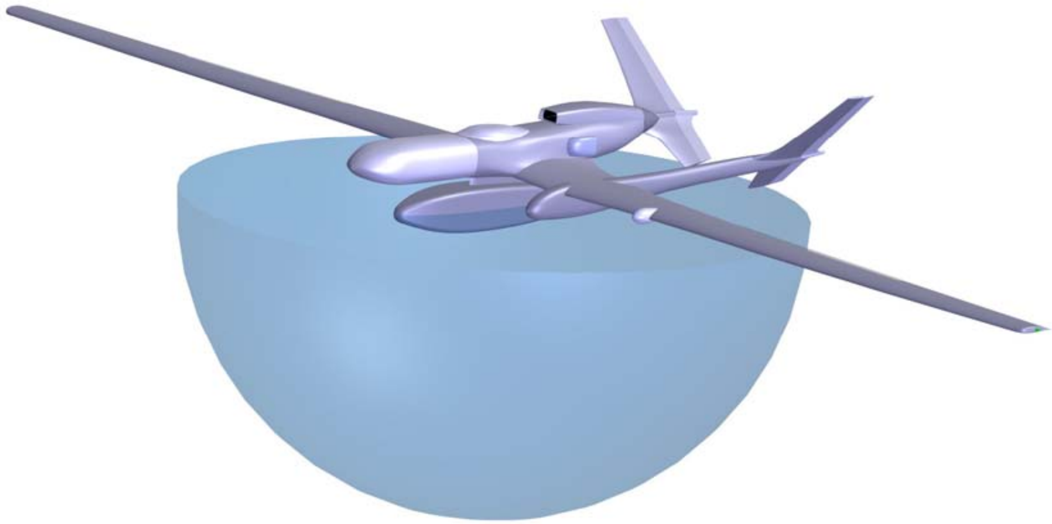

Figure 33 – Underslung Customer-Configured Payload

A set of other benefits is contained in the under-fuselage mounting shown. The customer is afforded a high degree of modularity and simplicity of integration by not being limited by the materials and spatial constraints of the aircraft fuselage. By creating a custom fairing for the payload, a science package can easily be carried underneath the aircraft. For this reason, such a payload carriage option is a much preferred choice by the many customers of the *Proteus* manned High-Altitude research aircraft. The bulk of payloads carried by that aircraft are contained in such custom fairings. As can be seen from the illustration, the underslung payload possesses a 360° view of the ground below, making it an ideal location for earth-surface observation equipment such as radar or optical sensors.

16. RFP-Specified Systems

A set of clearances were specified in the RFP for all of the payload components of the aircraft. These clearances are described in Table 6 below.

Table 6 – Payload Clearances

System	Clearance Cone Boundaries
Dropsonde Container	45° Aft, 30° Sides, Down
Science Package	15° Below Horizon Sides, 45° Below Horizon Fore/Aft
Req'd Payload Bay/Satcom	15° Above Horizon Sides, 45° Above Horizon Fore/Aft
Weather Radar	FWD facing, 45° Sides, 15° Above Horizon, 45° Below Horizon.

The locations of these components in the aircraft can be seen to satisfy all the required clearance angles, and are illustrated in Figure 34 below.

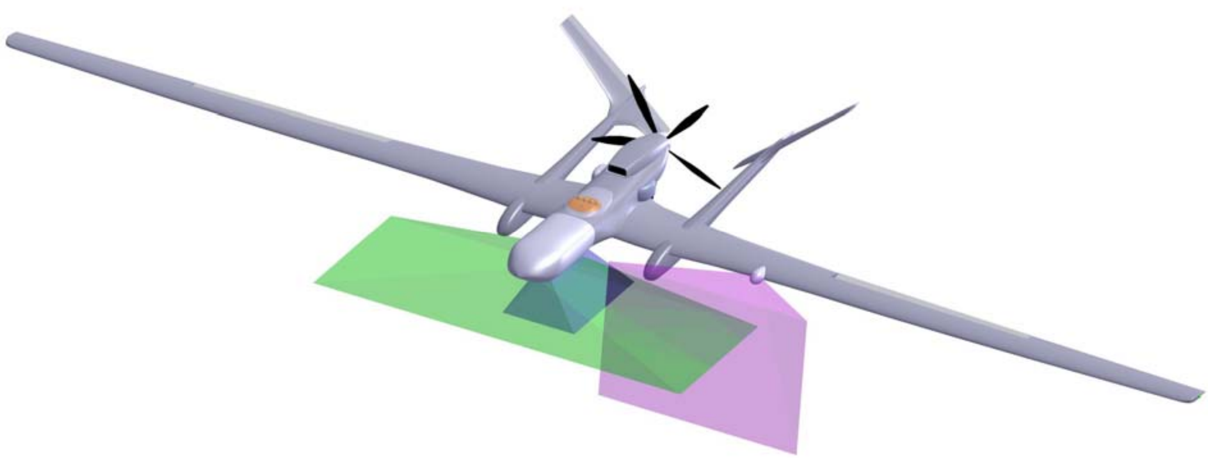

Figure 34 – RFP-Specified Systems Clearances

In picture above, the satcom antenna is outlined in orange inside its fairing on top of the fuselage. Its clearance is not shown for clarity, but it can be seen to easily satisfy and exceed the requirements of the RFP. Of additional interest is the weather radar, which is located in a fairing outboard of the fuselage on the port wing. In order to maintain the complete modularity of the payload section, the traditional "nose" location of such an integral system component would not be possible. However, considering the low-precision data acquired from this sensor, the asymmetric location of the weather radar is unlikely to cause any difficulties.

A system to combat ice formation that is necessary on any aircraft whose mission may place it in adverse weather conditions. *Adamant* employs the Low Power Ice Protection System, a recent development by Cox & Company, Inc. This system uses less power than current surface-heating anti-icing systems and also allows for a much more aerodynamically efficient installation than "inflatable boot" deicing systems. The anti-icing element of the system heats the leading edge of the airfoil, preventing ice from forming. Past the leading edge, the Electro-Mechanical Expulsion Deicing System (EMEDS) functions to break up and remove ice.[9] This system is envisioned installed on the leading edges of the wings, control surfaces, propeller and the engine intake. Another concern that needs to be mitigated is the ice ingestion by the engine intake. An intake particle separator is likely to be easy to integrate into the intake system to safeguard against any ice particles that may enter the intake after being separated from the intake lip.

17. System Operations

17.1 Vehicle Control

Establishing the mission control requirements for the aircraft required a detailed evaluation of the RFP mission. The direct in-situ weather research component of the mission would not likely be performed by an aircraft operating autonomously. Because of the unpredictable, quickly-changing conditions present inside a hurricane, it is doubtful that a fully-autonomous aircraft could have the sufficient situational awareness or control logic. The long-endurance loiter part of the mission can certainly benefit from an increase in system autonomy enabling operators to function more as mission controllers rather than flight crew, only taking over control for the data gathering/dropsonde deployment segment. However, the Concept of Operations which seems to best fit the mission specified in the RFP still requires direct control over the aircraft by human operators.

Using the above considerations, the UAV mission control level requirement was defined to be level 5 using TCS level definitions.[10] A requirement of the RFP is a Ku-band (12-18Ghz) dish antenna. The 2-ft diameter of the antenna specified allows the aircraft to maintain a duplex data link with the ground station, with the high frequency link providing the aircraft with plenty of bandwidth to send back sensor data in real-time. Every UAV had a set of distinct mission segments which may require different Command and Control (C^2) technologies. The design mission of *Adamant* requires the following control capabilities:

- Launch and Recovery – A short-range line-of-sight control which guides the aircraft during the takeoff and landing sequences. The LRE (Launch and Recovery Element) facilities are located at the launch site.

- Cruise to/from loiter area – This task is controlled by MCE (Mission Control Element) via the Satcom Ku-band link.
- Loiter– this is the primary mission of the MCE. A pilot and sensor operators control the aircraft and its sensors while loitering over the target.
- Data acquisition/sensor deployment – Judging from the RFP requirements, this segment will not occur within visual range of the LRE facilities and will have to be controlled by the mission control segment of the system. With the high bandwidth available via the Ku-band Satcom link, *Adamant* will be able to provide MCE with the information necessary to make a decision to attack.

A schematic of the communications scheme of the operations of the *Predator* system can be seen in Figure 35. With the significant similarity of the two missions, the operational scheme of the *Adamant* will be extremely similar to that of the *Predator*.

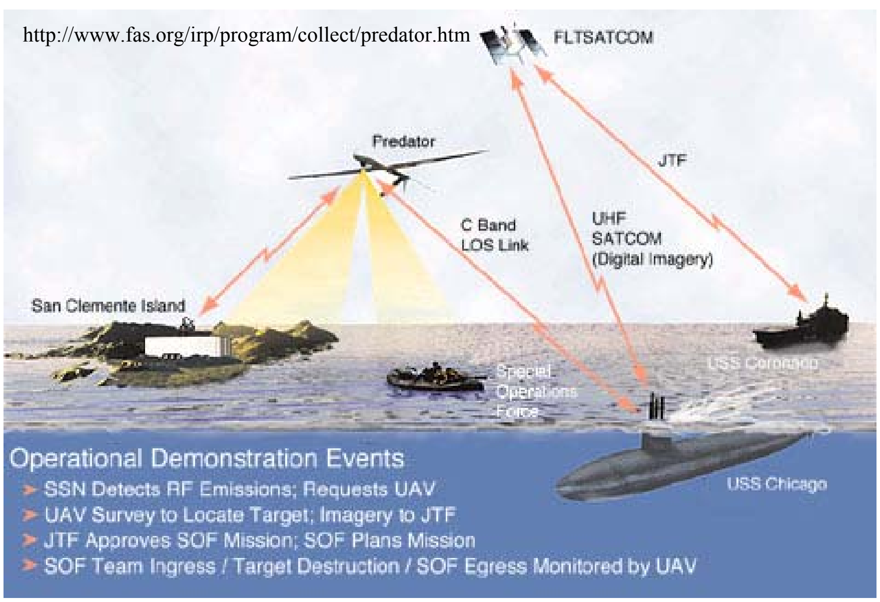

Figure 35 – Predator System Operational Schematic

The primary difference between the LRE and MCE is the lack of any wideband data links or image processing capability within the LRE and the addition of a Differential Global Positioning System (DGPS) system at the LRE to provide the precision navigation required for ground operations, take-off, and landing.[11]

To satisfy the control capabilities outlined previously, the aircraft needs to have multiple antennas. An omni-directional LOS antenna is required for the launch/recovery segment of flight. A directional link may be required for long-range line-of-sight communication, such as that encountered in climbing to cruise altitude or above weather which may be affecting Ku-band satcom operations. Finally, a long-distance over-the-horizon satcom antenna is required for control during cruise and loiter segments.

The delay present in the control execution is highly dependent on the communications technology used. Although during the loiter segment, the overall system lag requirement of the *Adamant* is <100 msec, there seems to not be any way to decrease the latency specifically for the data gathering/maneuvering segment where the requirement is the more constraining <40msec.[12] As such, the acceptable overall system lag is assumed to be <40msec for the long-distance control of *Adamant*. Since the communications are conducted through LEO satcom and/or line-of-sight systems, the system response time is high enough to not be of concern.

17.2 LEO Satcom Antenna

Most of modern long-range UAVs are controlled via LEO satcom systems, and operate those direct-line-of-sight links using parabolic antenna systems. A typical installation can be seen on the *Predator* UAV with a 32-inch parabolic antenna, which by the virtue of its installation takes up the majority of internal volume in the nose of the aircraft, significantly reducing available payload space and increasing the aircraft wetted area. This installation, shown in the *Predator A* UAV can be seen in Figure 36.

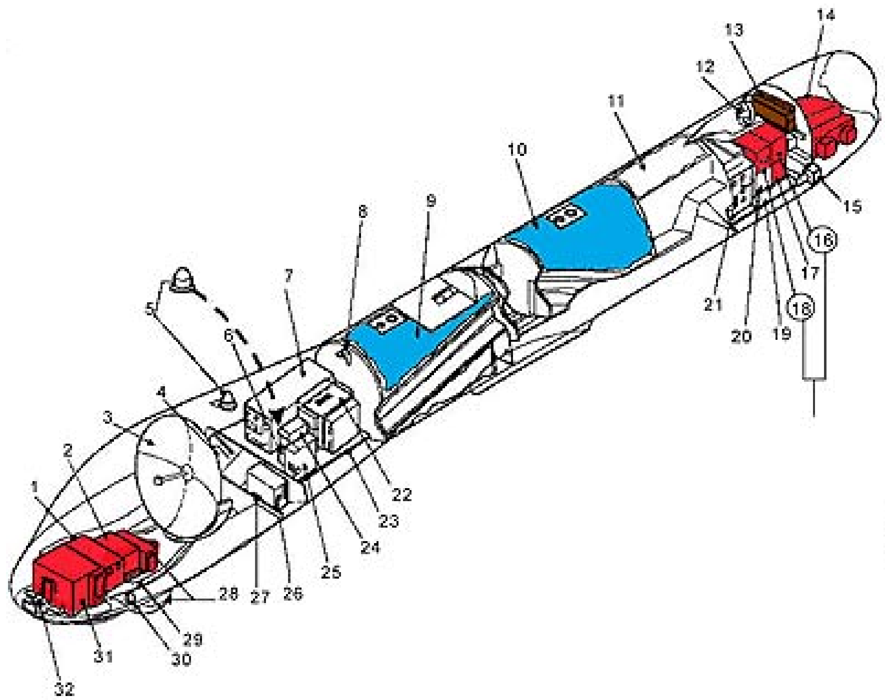

Figure 36 – Predator A Internals

The only notable exception to the parabolic-antenna installations is the *DarkStar* UAV, which used a flat-plate phased-array KU-band antenna, mounted on top of the aircraft's fuselage. The reason for this installation type and antenna choice were the LO requirements placed on the vehicle, the major downside is the significantly lower peak bandwidth and poor performance at low scanning angles, when compared to a parabolic. This type of antenna was considered to be unacceptable for use in *Adamant*, because the bandwidth would not be sufficient to ensure reliable real-time video transmission and aircraft control.

A third antenna option which combines the high bandwidth of a parabolic antenna with the easy low-drag installation of a phased-array system is a Luneberg Lens antenna.

Although invented in 1944, it is only recently that low-loss composites with tightly controlled dielectric constants and computer-design technology have enabled antennas of a consistent and high enough performance to be used for two-way communication.[13] Luneberg Lens antennas are currently used on commercial airliners to deliver internet and movie content to passengers, but Air Force Research Laboratory tests[14] have shown that such antennas allow two-way communications at performance levels equal to that of parabolic antennas of similar diameters. Because it has lower cost and higher performance than a phased-array antenna, while offering a much more compact installation than a parabolic, *Adamant* will use a Luneberg Lens antenna installed atop its fuselage to maintain a KU-Band communications link with the ground station.

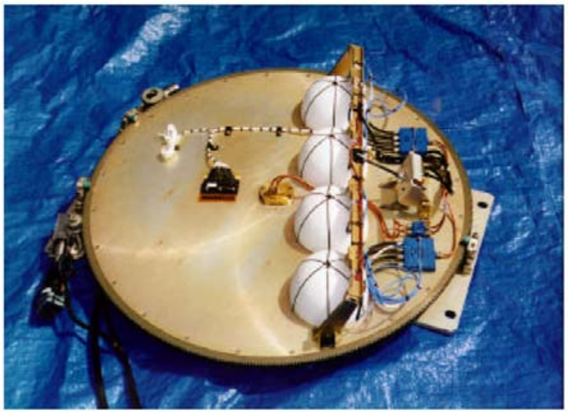

Figure 37 – Luneberg Lens Antenna

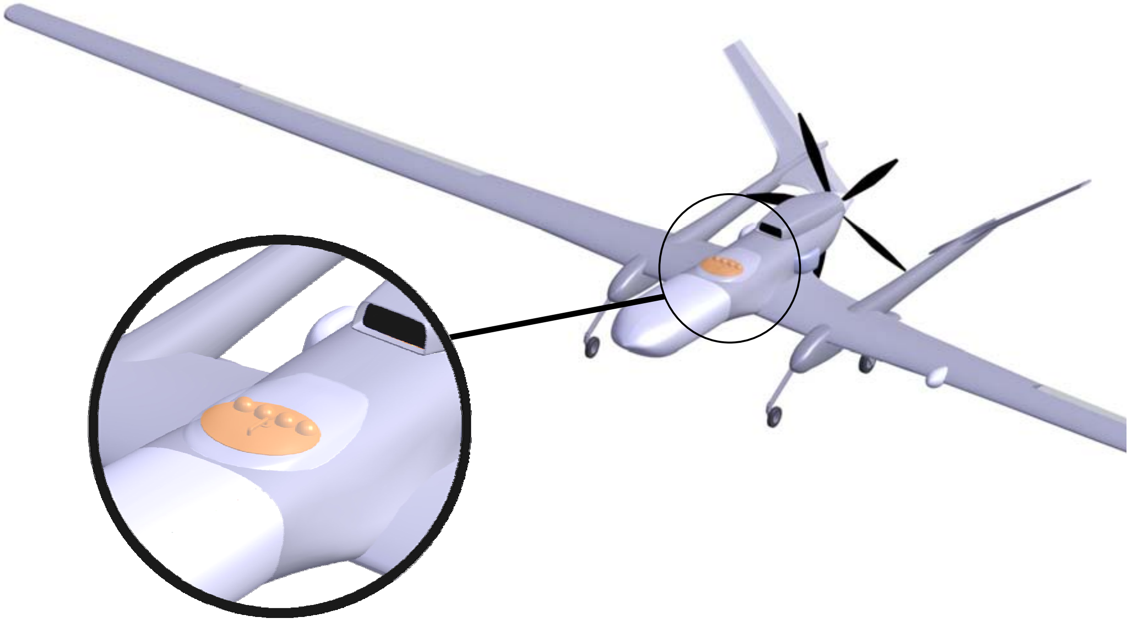

Figure 38 – Luneberg Lens Antenna Installation

17.3 System Deployment Considerations

Keeping in mind the one-piece construction of the airframe, the overall size of the aircraft, and the likely lack of high-capacity cargo aircraft in a civilian customer's possession, it was decided that it would not be advantageous to make *Adamant* deployable via cargo aircraft. Instead, in similarity to the *Global Hawk* platform and using the high range of the configuration, *Adamant* is designed to self-deploy most anywhere in the world. With *Adamant* possessing capability to operate in civilian airspace, this mission does not appear to be a difficult one. Although current FAA rules do not allow UAVs and manned aircraft to freely share space and fly in the same corridors, changes are likely to occur soon. The aircraft will be designed from the outset to be able to easily operate within the IFR flight environment in order to reduce costs required in future upgrades.

Because of its extremely high range, *Adamant* is easily deployable. In the example in figure 30 below, an *Adamant* system is shown to be able to self-deploy to any location in the world from just two bases: USA mainland and NSF Diego Garcia.

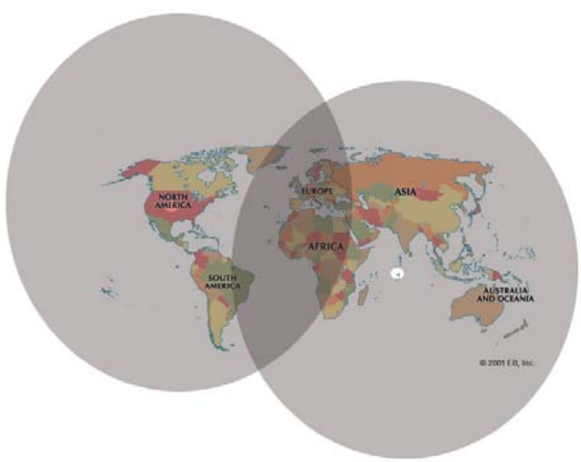

Figure 30 – 10,000+ nmi Deployment Radius

Adamant uses existing GCS equipment and technology of the *Predator* in order to decrease development costs. Using this GCS, *Adamant* can be controlled throughout its mission profile. Although with its 10,000 nmi range *Adamant* self-deploys to any part of the world, the L&R section of the system must be moved to the launch site by cargo aircraft. However, considering that *Adamant* operations will likely be conducted from a stationary mainland base, transportability of the L&R system is not of a large concern. Finally, the *Adamant* UAV will be designed to incorporate a "return home upon lost link" capability which should not present a significant level of technical difficulty.

The current UAV Ground Control Station (GCS) system used to control the *Predator* system is housed in a 30x8x8 foot, triple-axle, commercially available trailer. This trailer is not configured for air mobility and requires special handling to load and unload from C-130 and C-141 aircraft.[15]

Figure 31 – *Predator* System Ground Control Stations

The picture above right shows an alternative example of the more stationary deployment version of the Predator GCS system. It is very likely, that although mobile GCS systems are available, *Adamant* will be controlled via satellite from the customer's facility.

18. Cost Estimation

In order to estimate the costs of a production run of the *Adamant* system, cost methodologies from the DAPCA[16] cost estimation method were used. All of the costs estimated were updated to 2005 dollars using the standard Consumer Price Index[17]. No data were provided on the cost of the avionics, and those were estimated using a \$6,000/lb ratio suggested by the DAPCA cost method. A major concern with the RFP requirement is the specification that all cost calculations are to be performed for a 10-aircraft production run. Because this is an incredibly small buy lot for a relatively large airplane such as *Adamant*, it is impossible to make *Adamant* cost-competitive with other UAVs in the field. The effects of all of the development and engineering costs being amortized in just 10 vehicles can clearly be seen in Figure 39, where less than 25% of the estimated aircraft cost of \$41 million is made up of the actual aircraft manufacturing cost.

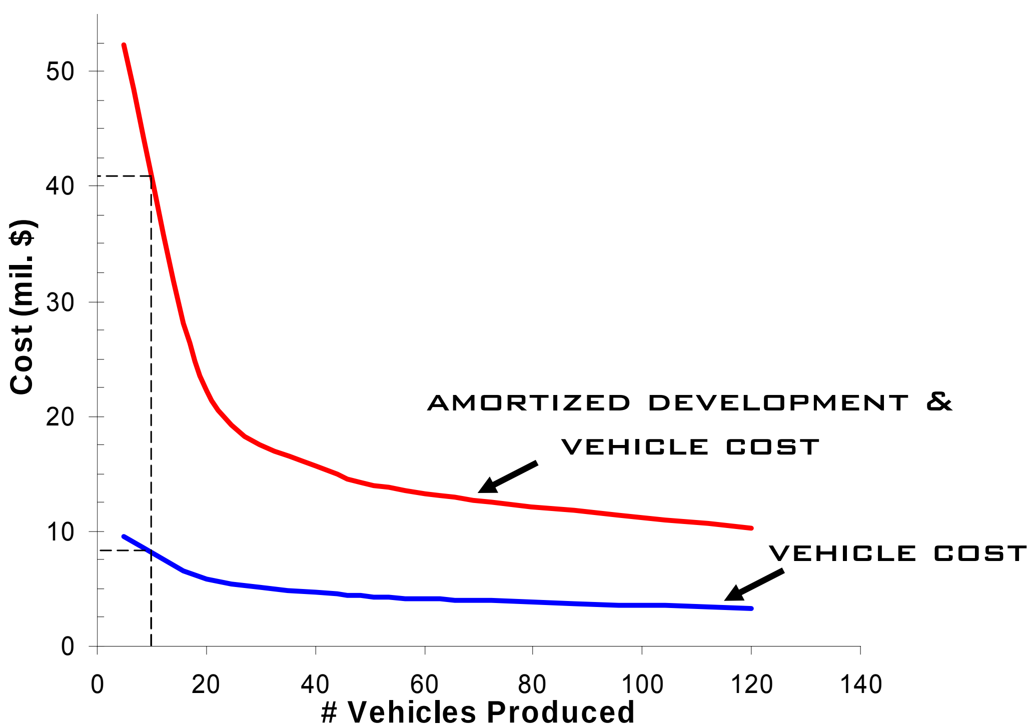

Figure 39 – Cost versus Production Run Size

Because other UAVs, such as the *Predator A* have production runs in excess of 100 vehicles, it is impossible to fairly compare their costs to the costs estimated for *Adamant*. With the apparent impossibility of making a 10-aircraft-buy be cost-competitive, the modular and mission-adaptable features of *Adamant* become doubly important, allowing the vehicle to be marketed to a variety of customers. Because its configuration enables *Adamant* to easily perform a variety of missions other than that specified in the RFP, the aircraft is sure to attract a wide variety of customers, increasing the overall buy size and dramatically decreasing per-vehicle costs.

Operating costs were calculated using the data and methods published in a report[18] by the RAND Corporation. The total cost of operating an aircraft fleet that maintains 2000 hours of loiter coverage in the mission specified by the RFP was calculated to be $5.7 million per year. This total operating cost is comprised of the cost of fuel, crew salary and maintenance cost for the aircraft, with the per-year cost breakdown being shown below in Table 7. All the salary costs shown are “wrap rates”, which include the cost of direct salaries paid to employees as well as the employee benefits, overhead and administrative costs. It can be seen that the cost for a 5-year mission would be approximately $23 million.

Table 7 – Operations Costs Breakdown

Fuel	2,917	hrs
	224,422	gal
	$789,249	
crew salary/hr	$1152	/hr
	$3,938,918	
maintenance	$283	/hr
	$ 967,575	
Total Ops Cost	**$5,695,742**	**/year**

19. Validation Model

An electric-powered validation model of the design was manufactured by hand from a variety of composite materials. A number of goals motivated the creation of this a model. The most important one was the evaluation of controllability and flight characteristics of the full-scale design. A set of secondary issues that the model would answer ranged from ground handling and landing performance to the amount of pitch-down moment imparted by the retracted landing gear. Powered by a lithium-polymer propulsion pack and a brushless Hacker B-40L motor, the model uses a 10x9 two-bladed propeller to attain upwards of 150 watts of peak power.

Figure 40 – Validation Model

The spar sizing code developed for the full-scale aircraft was used to size the spar for the scale model. The wing was manufactured using a hot-wired foam core with unidirectional carbon-fiber spar caps and fiberglass skins. Carbon fiber tube-and-rod wing joiners allowed for the aircraft's wing to split in order to simplify the transport of the model. The remainder of the model was manufactured using wet lay-up methods using fiberglass and carbon fiber composite materials.

Although it would be have been desirable to create a validation model to match the in-mission Reynolds number of the full-size aircraft, that task proved to be extremely difficult. In order to match the lowest full-scale in-mission Reynolds number (at the 65,000ft loiter point), a fast-flying RC model with a wingspan of approximately 25 feet would have to be created. This goal proved to be unfeasible both monetarily and technically, and a 7.5% scale model was created instead, with no Reynolds-number matching attempted. This model can be seen in Figure 40.

A collage of video captures from the first test flight of *Adamant* can be seen in Figure 41.

Figure 41 – Flight Testing Video Captures

Flight testing of the *Adamant* scale model resulted in a number of valuable finds. Most importantly, the aircraft was demonstrated to be easily controllable in all phases of flight, by taking off, flying a mission, and landing without sustaining major damage. The aircraft was noticed to have relatively low pitch stability and damping, owing to the high dihedral of the V-tail segments. Considerable increase in directional stability was noticed with the application of power – a characteristic expected of a pusher aircraft like *Adamant*. Nonetheless, the aircraft was stable and controllable even with an idling propeller – if it becomes necessary, it is certain that controllability characteristics of the full-scale aircraft could be improved by an integration of a rudimentary flight stability system.

After evaluation of the flight characteristics of the scale model, a number of changes were made to the overall design, with the most important one being the dihedral angle of the V-tails. The dihedral angle was decreased from that used on the RC model to the final iteration of the design, presented in this current report. This increased both the horizontal damping and pitch stability, at the expense of vertical damping/yaw stability components which were found to be sufficiently high to allow a degree of decrease.

The scale model proved to be both an exciting and useful way to bring a paper-only design competition to life. The model provided useful performance and controllability information and prompted a number of changes to the design. In addition to all this, the model will prove to be a wonderful addition to the designer's living room ceiling for years to come.

20. Conclusion

In this age of intensive spending on military and declining scientific budgets, the task of developing a purely scientific vehicle faces many difficulties beyond the technical. Finding the monetary support to develop a brand-new high-capability UAV may prove impossible if this vehicle is designed for one specific task and customer. With this constraint in mind, it is vital to attract as many customers as possible to such a development, both by the vehicle performance and by its modularity and adaptability to different missions.

The design of *Adamant* answers the mission of the 2004-2005 AIAA Individual Aircraft Design RFP in a simple high-performance vehicle, using proven and mature technologies. The aircraft incorporates a number of novel design choices, ranging from the twin-engine safety of its engine system to the easily-removable nose payload section and the clear, easily-accessibly underbody. With the good aerodynamic characteristics afforded to it by the pusher engine installation, tail surface configuration and the low-drag satcom antenna installation, *Adamant* maximizes the performance for the RFP mission. The aircraft meets or exceeds all of the requirements of the RFP with the exception of the ultimate G-load requirement, which was judged as excessive for the mission. The degree of compliance to the requirements of the RFP can be seen in Table 8.

Table 8 – RFP Requirements Compliance Matrix

RFP Requirement	Quantity	Note	Met?
Cruise range	1500nmi		✓
Dash-in Minimum Speed	200kts		✓
Balanced Field Length	5,500ft		✓
Service Ceiling	65,000ft	only light mission	✓
Ultimate load	+9/-6G	Challenge RFP	🚫
Existing Propulsion System	N/A		✓
Mission modularity		Removable 'nose'	✓

Adamant is a highly integrated, but easily modifiable multi-mission aircraft that combines a number of innovative off-the-shelf technologies in a synergistic manner. The aircraft can perform weather reconnaissance and other high-altitude long-endurance missions for both civilian and military customers at a low cost, with high safety and efficiency. *Adamant* presents an excellent solution to the mission of the 2004-2005 AIAA Individual Aircraft Design Competition, offering flight performance and features unrivaled by any other UAV in the world.

Appendix 1

T-56
scaled 2700

Altitude	Mach	Fn - net thrust	sfc	Power
0	0	530.6	0.51	2700.0
0	0	506.2	0.51	2696.5
0	0.1	458.1	0.53	2710.0
0	0.1	435.1	0.53	2706.3
0	0.2	392.7	0.51	2769.8
0	0.2	368.7	0.51	2766.3
0	0.3	332.0	0.50	2881.2
0	0.3	306.8	0.50	2877.9
0	0.4	278.6	0.49	3026.0
0	0.4	254.5	0.49	3022.9
0	0.5	240.7	0.48	3073.2
0	0.5	215.5	0.48	3070.6
0	0.6	218.9	0.48	3074.6
0	0.6	189.9	0.48	3072.0
0	0.7	213.1	0.48	3079.5
0	0.7	177.9	0.48	3076.9
0	0.8	223.5	0.49	3061.4
0	0.8	179.4	0.49	3058.6
5000	0	475.6	0.50	2425.1
5000	0	451.2	0.50	2421.8
5000	0.1	413.6	0.51	2450.6
5000	0.1	390.3	0.51	2447.3
5000	0.2	358.3	0.50	2502.1
5000	0.2	334.3	0.50	2499.0
5000	0.3	306.9	0.48	2597.4
5000	0.3	283.7	0.48	2594.5
5000	0.4	261.6	0.47	2734.1
5000	0.4	238.4	0.47	2731.2
5000	0.5	224.9	0.46	2844.6
5000	0.5	201.9	0.46	2841.7
5000	0.6	198.1	0.46	2956.1
5000	0.6	171.4	0.46	2953.2
5000	0.7	181.2	0.45	3119.3
5000	0.7	148.6	0.45	3116.6
5000	0.8	174.2	0.45	3134.9
5000	0.8	133.7	0.45	3132.1
10000	0	420.6	0.49	2179.9
10000	0	396.1	0.49	2177.0
10000	0.1	369.1	0.50	2196.3
10000	0.1	345.5	0.50	2193.4
10000	0.2	323.9	0.49	2232.8
10000	0.2	299.9	0.49	2230.1
10000	0.3	281.7	0.47	2312.7
10000	0.3	260.5	0.47	2310.1
10000	0.4	244.6	0.46	2439.3
10000	0.4	222.3	0.46	2436.6
10000	0.5	209.2	0.45	2583.2
10000	0.5	188.4	0.45	2580.3
10000	0.6	177.3	0.44	2756.5
10000	0.6	152.9	0.44	2753.5
10000	0.7	149.2	0.43	2998.2
10000	0.7	119.3	0.43	2995.5
10000	0.8	124.9	0.43	3060.6
10000	0.8	87.9	0.43	3057.9
15000	0	371.9	0.51	1979.5
15000	0	355.1	0.51	1977.5
15000	0.1	327.6	0.50	1945.4
15000	0.1	306.4	0.50	1943.0
15000	0.2	288.7	0.49	1953.4
15000	0.2	265.0	0.49	1950.9
15000	0.3	253.5	0.47	2018.3
15000	0.3	231.7	0.47	2015.8
15000	0.4	223.3	0.46	2133.6
15000	0.4	202.5	0.46	2131.1
15000	0.5	196.5	0.44	2275.3
15000	0.5	176.9	0.44	2272.6
15000	0.6	173.0	0.43	2451.0
15000	0.6	150.7	0.43	2448.3
15000	0.7	151.2	0.42	2669.3
15000	0.7	126.2	0.42	2666.7
15000	0.8	134.0	0.42	2807.3
15000	0.8	102.4	0.42	2804.9
20000	0	323.2	0.52	1778.7
20000	0	314.1	0.52	1777.6
20000	0.1	286.1	0.50	1703.0
20000	0.1	267.3	0.50	1701.1
20000	0.2	253.4	0.48	1689.3
20000	0.2	230.2	0.48	1687.0
20000	0.3	225.2	0.47	1740.7
20000	0.3	203.0	0.47	1738.4
20000	0.4	202.0	0.45	1840.6
20000	0.4	182.8	0.45	1838.3
20000	0.5	183.7	0.44	1962.5
20000	0.5	165.3	0.44	1960.1
20000	0.6	168.7	0.43	2113.7
20000	0.6	148.4	0.43	2111.4
20000	0.7	153.3	0.42	2273.3

20000	0.7	133.2	0.42	2271.0
20000	0.8	143.1	0.41	2468.7
20000	0.8	116.9	0.41	2466.6
25000	0	289.8	0.52	1512.9
25000	0	281.5	0.52	1511.9
25000	0.1	254.3	0.50	1471.9
25000	0.1	239.7	0.50	1470.3
25000	0.2	224.1	0.48	1472.5
25000	0.2	206.1	0.48	1470.7
25000	0.3	199.0	0.46	1515.1
25000	0.3	181.0	0.46	1513.3
25000	0.4	179.4	0.45	1589.2
25000	0.4	162.9	0.45	1587.2
25000	0.5	165.0	0.44	1689.4
25000	0.5	149.6	0.44	1687.4
25000	0.6	153.8	0.42	1819.8
25000	0.6	137.1	0.42	1817.8
25000	0.7	143.9	0.41	1955.0
25000	0.7	130.1	0.41	1953.1
25000	0.8	137.8	0.41	2128.7
25000	0.8	122.3	0.41	2126.8
30000	0	256.3	0.51	1256.1
30000	0	248.8	0.51	1255.0
30000	0.1	222.6	0.50	1256.5
30000	0.1	212.0	0.50	1255.4
30000	0.2	194.7	0.48	1273.6
30000	0.2	182.1	0.48	1272.4
30000	0.3	172.7	0.46	1307.3
30000	0.3	159.1	0.46	1306.0
30000	0.4	156.9	0.45	1355.9
30000	0.4	143.0	0.45	1354.4
30000	0.5	146.4	0.43	1433.5
30000	0.5	133.9	0.43	1431.8
30000	0.6	138.9	0.42	1540.0
30000	0.6	125.8	0.42	1538.4
30000	0.7	134.4	0.41	1655.6
30000	0.7	126.9	0.41	1653.9
30000	0.8	132.5	0.40	1785.4
30000	0.8	127.8	0.40	1783.7
35000	0	225.3	0.51	1080.5
35000	0	200.4	0.51	1080.2
35000	0.1	197.7	0.49	1066.1
35000	0.1	176.4	0.49	1065.4
35000	0.2	175.0	0.48	1068.1
35000	0.2	156.6	0.48	1067.3
35000	0.3	157.1	0.46	1086.5
35000	0.3	141.0	0.46	1085.4
35000	0.4	144.3	0.45	1121.3
35000	0.4	129.8	0.45	1120.0
35000	0.5	136.1	0.43	1182.5
35000	0.5	122.7	0.43	1181.1
35000	0.6	131.3	0.42	1264.2
35000	0.6	117.5	0.42	1262.9
35000	0.7	129.4	0.41	1355.7
35000	0.7	117.6	0.41	1354.3
35000	0.8	129.9	0.40	1460.8
35000	0.8	119.6	0.40	1459.3
40000	0	194.3	0.51	926.4
40000	0	151.9	0.51	926.5
40000	0.1	172.8	0.49	889.4
40000	0.1	140.7	0.49	889.0
40000	0.2	155.3	0.48	873.1
40000	0.2	131.1	0.48	872.4
40000	0.3	141.5	0.46	877.7
40000	0.3	123.0	0.46	876.8
40000	0.4	131.6	0.45	903.0
40000	0.4	116.5	0.45	902.0
40000	0.5	125.7	0.43	950.0
40000	0.5	111.5	0.43	949.0
40000	0.6	123.6	0.42	1010.6
40000	0.6	109.1	0.42	1009.5
40000	0.7	124.4	0.41	1080.6
40000	0.7	108.2	0.41	1079.5
40000	0.8	127.4	0.40	1167.0
40000	0.8	111.5	0.40	1165.8
45000	0	197.7	0.51	753.4
45000	0	160.4	0.51	753.2
45000	0.1	175.6	0.49	717.1
45000	0.1	147.0	0.49	716.7
45000	0.2	157.4	0.48	698.4
45000	0.2	135.6	0.48	697.8
45000	0.3	143.3	0.46	697.3
45000	0.3	126.2	0.46	696.5
45000	0.4	133.0	0.45	713.9
45000	0.4	118.8	0.45	713.1
45000	0.5	126.9	0.43	746.9
45000	0.5	113.5	0.43	746.1
45000	0.6	124.4	0.42	795.5
45000	0.6	110.6	0.42	794.7
45000	0.7	125.0	0.41	851.6
45000	0.7	109.9	0.41	850.7
45000	0.8	127.7	0.40	925.8
45000	0.8	113.0	0.40	924.9
50000	0	201.2	0.51	575.0
50000	0	169.0	0.51	574.0
50000	0.1	178.4	0.50	552.5
50000	0.1	153.3	0.50	551.7
50000	0.2	159.6	0.48	540.8
50000	0.2	140.1	0.48	540.1
50000	0.3	145.0	0.46	539.8

50000	0.3	129.4	0.46	539.3
50000	0.4	134.4	0.45	549.6
50000	0.4	121.2	0.45	549.0
50000	0.5	128.0	0.44	569.5
50000	0.5	115.4	0.44	568.9
50000	0.6	125.3	0.42	613.6
50000	0.6	112.1	0.42	613.1
50000	0.7	125.5	0.41	661.6
50000	0.7	111.5	0.41	660.9
50000	0.8	128.0	0.40	730.0
50000	0.8	114.4	0.40	729.4
55000	0	204.6	0.52	391.1
55000	0	177.5	0.52	388.7
55000	0.1	181.1	0.50	395.4
55000	0.1	159.6	0.50	393.9
55000	0.2	161.8	0.48	400.1
55000	0.2	144.6	0.48	399.4
55000	0.3	146.7	0.47	405.3
55000	0.3	132.6	0.47	404.9
55000	0.4	135.8	0.45	410.1
55000	0.4	123.5	0.45	409.8
55000	0.5	129.2	0.44	417.9
55000	0.5	117.4	0.44	417.4
55000	0.6	126.1	0.43	464.9
55000	0.6	113.5	0.43	464.6
55000	0.7	126.1	0.42	510.5
55000	0.7	113.2	0.42	510.1
55000	0.8	128.3	0.41	579.7
55000	0.8	115.8	0.41	579.3
60000	0	208.1	0.52	201.9
60000	0	186.1	0.52	197.4
60000	0.1	183.9	0.50	245.9
60000	0.1	165.9	0.50	243.4
60000	0.2	164.0	0.48	276.5
60000	0.2	149.1	0.48	275.5
60000	0.3	148.5	0.47	293.7
60000	0.3	135.7	0.47	293.4
60000	0.4	137.2	0.45	295.5
60000	0.4	125.8	0.45	295.5
60000	0.5	130.3	0.44	292.0
60000	0.5	119.4	0.44	291.7
60000	0.6	127.0	0.43	349.2
60000	0.6	115.0	0.43	349.1
60000	0.7	126.6	0.42	398.4
60000	0.7	114.8	0.42	398.2
60000	0.8	128.5	0.41	474.7
60000	0.8	117.3	0.41	474.6
65000	0	211.5	0.52	7.2
65000	0	194.7	0.52	0.1
65000	0.1	186.7	0.51	104.0
65000	0.1	172.2	0.51	100.2
65000	0.2	166.2	0.49	170.0
65000	0.2	153.6	0.49	168.5
65000	0.3	150.2	0.47	205.0
65000	0.3	138.9	0.47	204.9
65000	0.4	138.6	0.46	205.8
65000	0.4	128.2	0.46	206.0
65000	0.5	131.5	0.44	191.9
65000	0.5	121.4	0.44	191.6
65000	0.6	127.8	0.43	266.7
65000	0.6	116.5	0.43	266.9
65000	0.7	127.2	0.43	325.2
65000	0.7	116.5	0.43	325.3
65000	0.8	128.8	0.42	415.1
65000	0.8	118.7	0.42	415.3
70000	0	215.0	0.53	-193.0
70000	0	203.2	0.53	-203.3
70000	0.1	189.4	0.51	-30.4
70000	0.1	178.5	0.51	-35.8
70000	0.2	168.4	0.49	80.4
70000	0.2	158.1	0.49	78.4
70000	0.3	151.9	0.47	139.3
70000	0.3	142.1	0.47	139.3
70000	0.4	140.0	0.46	140.9
70000	0.4	130.5	0.46	141.3
70000	0.5	132.6	0.45	117.5
70000	0.5	123.3	0.45	117.2
70000	0.6	128.7	0.44	217.4
70000	0.6	118.0	0.44	217.7
70000	0.7	127.7	0.43	291.0
70000	0.7	118.1	0.43	291.3
70000	0.8	129.1	0.43	400.9
70000	0.8	120.1	0.43	401.4

Appendix 2

```
Adamant, AVL input file
0.0                  !   Mach
0     0     0.0      !   iYsym  iZsym  Zsym
380.0 5.5 100.0      !   Sref   Cref   Bref   reference area, chord, span
3.00  0.0   0.5      !   Xref   Yref   Zref   moment reference location (arb.)
0.020                !   CDp
#
#==============================================
BODY
Fuselage
12  1.0
#
TRANSLATE
-11.0  0.0  1.0
#
SCALE           |  (keyword)
1.0  1.0  1.0
#
BFIL
fuseAD.dat
#==============================================
BODY
Boom1
12  1.0
#
TRANSLATE
-1.0  7.25  -.75
#
SCALE           |  (keyword)
0.9  0.7  0.7
#
BFIL
fuseAD.dat
#==============================================
BODY
Boom2
12  1.0
#
TRANSLATE
-1.0  -7.25  -.75
#
SCALE           |  (keyword)
0.9  0.7  0.7
#
BFIL
fuseAD.dat
#============================================================
#
SURFACE                    | (keyword)
Wing
#Nchord    Cspace   [ Nspan Sspace ]
 10        1.0
```

```
INDEX                  | (keyword)
111                    | Lsurf

YDUPLICATE
0.0

SCALE
1.0  1.0  1.0

TRANSLATE
0.0  0.0  0.0

ANGLE
0.0                    | dAinc

#____________________________________
SECTION                                  |  (keyword)
  0.00    0.00    0.00    7.00  0.0    4    2   | Xle Yle Zle   Chord Ainc   [ Nspan Sspace ]

AFIL 0.0 1.0
E431.dat

#_______________
SECTION                                  |  (keyword)
  1.16   10.00   -0.52    4.50 -1.5   16   -2   | Xle Yle Zle   Chord Ainc   [ Nspan Sspace ]

AFIL 0.0 1.0
E431.dat

#Cname   Cgain  Xhinge  HingeVec      SgnDup
CONTROL
aileron  1.0   0.6     0.0 0.0 0.0    -1.0

#_______________
SECTION                                  |  (keyword)
  2.11   50.00   -0.52    2.00 -1.8    8   -2   | Xle Yle Zle   Chord Ainc   [ Nspan Sspace ]

AFIL 0.0 1.0
E431.dat

#Cname   Cgain  Xhinge  HingeVec      SgnDup
CONTROL
aileron  1.0   0.6     0.0 0.0 0.0    -1.0
#
#==============================================================
#
SURFACE
V-tail
5  1.0
YDUPLICATE
    0.00000
ANGLE
   0.000
TRANSLATE
   17.00000     6.20000     -1.30
```

```
#---------------------------
#   Xle       Yle       Zle       chord      angle   Nspan  Sspace
SECTION
    1.15000    -2.2000    -3.3000    2.4        0.000   7     -1.5

AFIL 0.0 1.0
naca0012.dat

#so left tail is defined, since Y-axis is positive out the right wingtip
#tail is defined bottom section, middle section, top section

#Cname   Cgain  Xhinge  HingeVec      SgnDup
CONTROL
elevator  1.0   0.6     0.0 0.0 0.0    1.0
CONTROL
rudder   -1.0   0.6     0.0 0.0 0.0    -1.0
#---------------------------
#   Xle       Yle       Zle       chord      angle   Nspan  Sspace
SECTION
    0.00000    0.0000     0.0000     3.65       0.000   7     -1.5

AFIL 0.0 1.0
naca0012.dat

#Cname   Cgain  Xhinge  HingeVec      SgnDup
CONTROL
elevator  1.0   0.7     0.0 0.0 0.0    1.0
CONTROL
rudder   -1.0   0.7     0.0 0.0 0.0    -1.0
#---------------------------
SECTION
    1.2       4.5       6.0000     2.14       0.000   7     -1.5

AFIL 0.0 1.0
naca0012.dat

CONTROL
elevator  1.0   0.63    0.0 0.0 0.0    1.0
CONTROL
rudder   -1.0   0.63    0.0 0.0 0.0    -1.0
#
#==============================================
```

References

[1] "FLIGHT DEMONSTRATIONS EVALUATE UAV COLLISION-AVOIDANCE TECHNOLOGY" http://www.nasa.gov/centers/dryden/news/NewsReleases/2003/03-20_pf.html

[2] KENDALL, E. R. (Gates Learjet Corp., Wichita, KS) AIAA-1984-2164 American Institute of Aeronautics and Astronautics, Applied Aerodynamics Conference, 2nd, Seattle, WA, Aug. 21-23, 1984. 11 p.

[3] XFLR – http://www.geocities.com/xflr5/xflr5.htm

[4] XFOIL – http://raphael.mit.edu/xfoil/ - Mark Drela (drela@mit.edu), Harold Youngren (guppy@maine.com)

[5] Roger D. Schaufele, *The Elements of Aircraft Preliminary Design,* ARIES Publications, Santa Ana, CA, 2000.

[6] JavaProp – http://www.mh-aerotools.de/airfoils/javaprop.htm – © *2004 Martin Hepperle*

[7] Airplane Design, Vol. V, Dr. Jan Roskam, ISBN: 1-884885-24-1

[8] Aircraft Design: A Conceptual Approach Third Edition, Daniel P. Raymer, ISBN 1-56347-281-0, P. 587, page 406

[9] http://www.techbriefs.com/spinoff/spinoff2002/ps_1.html

[10] http://www.fas.org/irp/program/collect/uav_tcs.htm

[11] http://www.fas.org/irp/doddir/usaf/conops_uav/part02.htm

[12] http://www.ae.utexas.edu/ASE261Kchaput/Lesson9.ppt

[13] http://www.afcea.org/signal/articles/anmviewer.asp?a=411&z=80

[14] "An Airborne Global Broadcast Service/Military Strategic and Tactical Relay Satellite Wideband Antenna", Air Force Research Laboratory, http://www.afrlhorizons.com/Briefs/0009/IF9906.html

[15] http://www.fas.org/irp/program/collect/uav_gcs.htm

[16] Aircraft Design: A Conceptual Approach Third Edition, Daniel P. Raymer, ISBN 1-56347-281-0, P. 587

[17] CPI - http://minneapolisfed.org/Research/data/us/calc/hist1913.cfm

[18] Hess, R.W., and Romanoff, H.P., "Aircraft Airframe Cost Estimating Relationships," Rand Corporation, Rept. R-3255-AF, Santa Monica, CA, 1987

Other Sources

- Aircraft Design for the New Millenium, Darold B. Cummings, David W. Hall, P.E., Cal Poly San Luis Obispo, CA

- The Design of the Airplane, Darrol Stinton, AIAA, ISBN 0-632-01877-1